CrossMark

J. Fluid Mech. (2018), *vol.* 840, *pp.* 656–687. © Cambridge University Press 2018
doi:10.1017/jfm.2018.88

Dynamics of capsules enclosing viscoelastic fluid in simple shear flow

Zheng Yuan Luo[1] **and Bo Feng Bai**[1,†]

[1]State Key Laboratory of Multiphase Flow in Power Engineering, Xi'an Jiaotong University, Xi'an 710049, China

(Received 16 February 2017; revised 12 December 2017; accepted 16 January 2018; first published online 14 February 2018)

Previous studies on capsule dynamics in shear flow have dealt with Newtonian fluids, while the effect of fluid viscoelasticity remains an unresolved fundamental question. In this paper, we report a numerical investigation of the dynamics of capsules enclosing a viscoelastic fluid and which are freely suspended in a Newtonian fluid under simple shear. Systematic simulations are performed at small but non-zero Reynolds numbers (i.e. $Re = 0.1$) using a three-dimensional front-tracking finite-difference model, in which the fluid viscoelasticity is introduced via the Oldroyd-B constitutive equation. We demonstrate that the internal fluid viscoelasticity presents significant effects on the deformation behaviour of initially spherical capsules, including transient evolution and equilibrium values of their deformation and orientation. Particularly, the capsule deformation decreases slightly with the Deborah number De increasing from 0 to $O(1)$. In contrast, with De increasing within high levels, i.e. $O(1–100)$, the capsule deformation increases continuously and eventually approaches the Newtonian limit having a viscosity the same as the Newtonian part of the viscoelastic capsule. By analysing the viscous stress, pressure and viscoelastic stress acting on the capsule membrane, we reveal that the mechanism underlying the effects of the internal fluid viscoelasticity on the capsule deformation is the alterations in the distribution of the viscoelastic stress at low De and its magnitude at high De, respectively. Furthermore, we find some new features in the dynamics of initially non-spherical capsules induced by the internal fluid viscoelasticity. Particularly, the transition from tumbling to swinging of oblate capsules can be triggered at very high viscosity ratios by increasing De alone. Besides, the critical viscosity ratio for the tumbling-to-swinging transition is remarkably enlarged with De increasing at relatively high levels, i.e. $O(1–100)$, while it shows little change at low De, i.e. below $O(1)$.

Key words: biological fluid dynamics, capsule/cell dynamics

1. Introduction

To understand the mechanical behaviour of an individual capsule in shear flow is an essential precondition for designing capsules and optimizing their functions as well as thoroughly understanding the rheology of capsule suspensions (Barthes-Biesel 2011; Forsyth *et al.* 2011; Barthes-Biesel 2016; Zhang *et al.* 2016). Therefore, the

† Email address for correspondence: bfbai@mail.xjtu.edu.cn

https://doi.org/10.1017/jfm.2018.88 Published online by Cambridge University Press

Category	**Composition**	**References**	
Newtonian capsules	Elastic membrane enclosing a Newtonian fluid	Reviews	Barthes-Biesel (2009, 2011, 2016), Finken, Kessler & Seifert (2011)
		Studies on initially spherical capsules	Barthes-Biesel (1980), Barthes-Biesel & Rallison (1981), Ramanujan & Pozrikidis (1998), Pozrikidis (2001), Barthes-Biesel *et al.* (2002), Lac *et al.* (2004), Lac & Barthes-Biesel (2005), Li & Sarkar (2008), Sui *et al.* (2009), Le (2010), Zhao & Bagchi (2011), Foessel *et al.* (2011), Yazdani & Bagchi (2013), Dupont *et al.* (2015), Matsunaga *et al.* (2015), Luo *et al.* (2015), de Loubens *et al.* (2016)
		Studies on initially non-spherical capsules	Kessler, Finken & Seifert (2008), Bagchi & Kalluri (2009), Walter, Salsac & Barthes-Biesel (2011), Vlahovska *et al.* (2011), Koleva & Rehage (2012), Omori *et al.* (2012), Cordasco & Bagchi (2013), Wang *et al.* (2013), Dupont, Salsac & Barthes-Biesel (2013), Villone *et al.* (2015), Dupont *et al.* (2016), Luo & Bai (2016)
Viscoelastic drops	Liquid interface enclosing a viscoelastic fluid	Yue *et al.* (2005*a*,*b*), Aggarwal & Sarkar (2007), Mukherjee & Sarkar (2009), Verhulst *et al.* (2009*a*,*b*), Guido (2011)	
Viscoelastic capsules	Elastic membrane enclosing a viscoelastic fluid	The present study	

TABLE 1. A brief list of literature relevant to the study of the deformation and dynamics of viscoelastic capsules in simple shear flow.

deformation and dynamical behaviours of capsules in shear flows have become an important branch subject in the discipline of fluid mechanics (see table 1 for relevant references). From the viewpoint of mechanics, the capsule dynamics is governed by the competition between the elastic stress in the membrane and the fluid stresses from the internal and external flows. Particularly, the external fluid stress induces capsule deformation, while the membrane stress and the internal fluid stress play a hindering role. These three competing forces can be characterized by two dimensionless parameters: the capillary number Ca (i.e. the ratio of the external fluid stress to the membrane stress) and the internal-to-external viscosity ratio λ_μ (i.e. the ratio of the internal to the external fluid stress). Barthes-Biesel and Rallison conducted the first studies on the capsule deformation using small-deformation analysis (Barthes-Biesel 1980; Barthes-Biesel & Rallison 1981). The capsule deformation is respectively

https://doi.org/10.1017/jfm.2018.88 Published online by Cambridge University Press

dominated by the membrane stress at $Ca \ll 1$ and the internal fluid stress at $\lambda_\mu \gg 1$, while in both cases the capsule deformation is quite small.

In most general cases, both the capillary number and the viscosity ratio turn out to be finite and hence capsules can undergo significant deformation, in which the coupling between the membrane stress and the fluid stresses becomes prominent. Consequently, the small-deformation analysis is no longer applicable and numerical approaches have received rapidly increasing attention. Note that the complex mechanics of the surrounding membrane (e.g. resistances against shear deformation, area dilatation and bending) is the principal feature distinguishing capsules from liquid drops having interfacial tension. Accordingly, so far the related studies have been primarily focused on the effects of the membrane mechanics, such as constitutive law, shear modulus, area dilatation, bending resistance, membrane viscosity and membrane prestress (Ramanujan & Pozrikidis 1998; Pozrikidis 2001; Barthes-Biesel *et al.* 2002; Lac *et al.* 2004; Lac & Barthes-Biesel 2005; Li & Sarkar 2008; Le 2010; Yazdani & Bagchi 2013; Dupont *et al.* 2015). Still, several studies have reported the critical effects of the flow condition which can cause obvious changes in both the internal and external fluid stresses, for example, oscillating shear flow or flow with non-negligible fluid inertia (Sui *et al.* 2009; Zhao & Bagchi 2011; Bai *et al.* 2013; Matsunaga *et al.* 2015). In the studies mentioned above, the viscosity ratio is usually restricted to unity or a few other values (e.g. 0.2 or 5). Foessel *et al.* (2011) systematically investigated the effects of the internal viscosity and found that the capsule deformation decreases significantly with the internal-to-external viscosity ratio, which may be attributed to the remarkably enlarged internal fluid stress. Recently, we studied the deformation of complex capsules with inhomogeneous internal medium (i.e. compound capsule). The presence of an inner capsule also inhibits the whole capsule deformation owing to the changes in the internal fluid stress induced by the hydrodynamic interactions between the inner and outer membranes (Luo *et al.* 2015). These studies have demonstrated that the internal fluid stress may play a critical role in the deformation and dynamics of capsules in shear flows.

Notably, all the reported studies on capsule dynamics are limited to capsules enclosing a Newtonian fluid inside (see table 1 for relevant references), which are appropriate models for red blood cells or artificial capsules with liquid internal contents such as water or aqueous solution. However, both in nature and in applications, there are many examples of capsules whose internal fluid exhibits a non-Newtonian fluid behaviour. For instance, many types of biological cells, e.g. white blood cells and circulating tumour cells, have much more complex internal structures than red blood cells, and hence their cytoplasm presents non-Newtonian behaviours (Tsai, Frank & Waugh 1993). The flow dynamics of those cells is fundamental to better understand their motion and function in physiological blood flow or microfluidic flows (Popel & Johnson 2005; Koumoutsakos, Pivkin & Milde 2013). In addition, some artificial capsules can also enclose a non-Newtonian fluid inside, for example, cell-like microcapsules harbouring biopolymers, proteins and other macromolecules inside their liquid cores, or capsules with a gelled core used for cell encapsulation or substance transport (Noble *et al.* 2004; Rożkiewicz, Myers & Stupp 2011; Huang *et al.* 2017). Understanding their mechanical behaviour in shear flows is also essential to help design and optimize these artificial capsules. Notably, compared with capsules enclosing a Newtonian fluid, the introduction of a non-Newtonian component into the internal fluid stress such as a viscoelastic stress will very likely cause significant changes in the mechanical behaviour of the whole capsule. The recent review on the motion and deformation of capsules in shear flows

https://doi.org/10.1017/jfm.2018.88 Published online by Cambridge University Press

by Barthes-Biesel (2016) has also clearly pointed out that the potential effect of the non-Newtonian internal medium is an important factor that needs to be considered. To the best of our knowledge, however, no study is available on the dynamics of capsules enclosing a non-Newtonian fluid.

Intensive studies have revealed the remarkable effects of the fluid viscoelasticity on the dynamics of liquid drops without a surrounding elastic membrane (see table 1 for relevant references). They are commonly limited to low Deborah numbers (e.g. $De \sim O(1)$) which are used to characterize the relative significance of the viscoelastic stress to the viscous stress. Evidently, the deformation and breakup of liquid drops are significantly affected by the presence of viscoelasticity in the surrounding fluid or the drop phase. The viscoelastic effect consists of two aspects: the direct impact of the viscoelastic stress at the drop interface and the alteration of the viscous stress from the Newtonian part owing to the viscoelasticity-induced flow modification (Ramaswamy & Leal 1999; Yue *et al.* 2005*b*). Particularly, the drop-phase viscoelasticity is found to slightly inhibit drop deformation, which is mainly attributed to the flow modification effect (Yue *et al.* 2005*b*; Aggarwal & Sarkar 2007). Similarly, for membrane-enclosed capsules with a viscoelastic fluid inside, the presence of the viscoelastic stress and its consequent effect on the flow field may also alter the coupling between the membrane stress and the internal and external fluid stresses, and hence significantly affects the flow dynamics of the whole capsule. Therefore, a systematic investigation is needed into the effects of the internal fluid viscoelasticity on the capsule dynamics.

In this paper, we study the deformation and dynamics of an individual capsule enclosing a viscoelastic fluid inside, which is freely suspended in a simple shear flow. Based on the three-dimensional front-tracking finite-difference method that we have developed previously for the study of capsules enclosing a Newtonian fluid (Luo *et al.* 2015; Luo & Bai 2016), the Oldroyd-B constitutive equation is further solved to take into account the internal fluid viscoelasticity. Using this model, we systematically investigate the effects of the internal fluid viscoelasticity on the deformation and tank-treading motion of an initially spherical capsule within a broad range of Deborah number, i.e. $De = 0$–100. Since an initially non-spherical capsule can present other types of unsteady dynamical motions, such as swinging and tumbling (see table 1 for relevant references), it is also of interest to examine the effects of the internal fluid viscoelasticity on the characteristics of the swinging and tumbling motions and their transition. Furthermore, we analyse the mechanisms underlying the effects of the fluid viscoelasticity in terms of the distribution and magnitude of the viscous and viscoelastic stresses acting on the capsule membrane.

2. Numerical methodology

2.1. *Problem description and mathematical formulation*

We consider the dynamics of an individual capsule consisting of a viscoelastic fluid enclosed by an elastic membrane (hereafter referred to as viscoelastic capsule) suspended in a Newtonian fluid under simple shear $\boldsymbol{u}_\infty = [\gamma z, 0, 0]$, where γ is the shear rate (see figure 1). The shear flow is generated by the movement of the upper and bottom plates with the same speed but in opposite directions. The coordinate system is set as follows: the x-axis is horizontal (i.e. parallel to the two plates) and is parallel to the flow direction; the y-axis is orthogonal to the x-axis and lies in the horizontal plane (i.e. the vorticity direction); and the z-axis is orthogonal to the two plates (i.e. the velocity gradient direction). The capsule is initially placed in the centre of the computational domain with a size of $L_x \times L_y \times L_z$ and remains as such owing

https://doi.org/10.1017/jfm.2018.88 Published online by Cambridge University Press

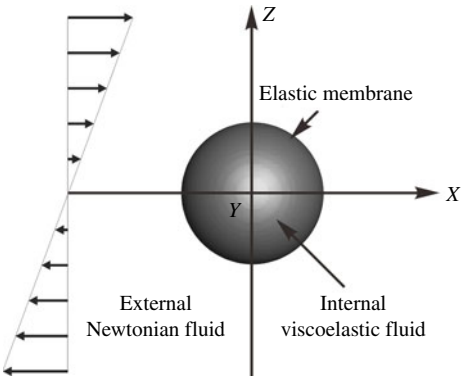


FIGURE 1. Problem statement. An individual capsule that consists of a viscoelastic fluid enclosed by an elastic membrane is freely suspended in a Newtonian fluid under simple shear. We study the dynamics of capsules with different initial configurations: a spherical shape and an oblate shape with the revolution axis in the shear plane.

to the symmetry of the whole flow system. Two different initial configurations of the capsule are considered: a spherical shape and an oblate shape with the revolution axis lying in the shear plane.

The flows of viscoelastic incompressible fluids are governed by the continuity and Navier–Stokes (NS) equations as follows:

$$\boldsymbol{\nabla}\cdot\boldsymbol{u}=0, \tag{2.1}$$

$$\frac{\partial(\rho\boldsymbol{u})}{\partial t}+\boldsymbol{\nabla}\cdot(\rho\boldsymbol{u}\boldsymbol{u})=-\boldsymbol{\nabla}p+\boldsymbol{\nabla}\cdot[\mu^s(\boldsymbol{\nabla}\boldsymbol{u}+\boldsymbol{\nabla}\boldsymbol{u}^{\mathrm{T}})+\boldsymbol{T}^p]+\boldsymbol{f}. \tag{2.2}$$

Here, $\boldsymbol{u}=(u,v,w)^{\mathrm{T}}$ is the fluid velocity vector, ρ is the fluid density, t is the time, p is the pressure and $\boldsymbol{f}$ is the body force resulting from the elastic stress in the membrane. μ^s is the solvent viscosity (i.e. the Newtonian part) and $\boldsymbol{T}^p$ is the extra stress tensor (or the viscoelastic stress) owing to the non-Newtonian part of the viscoelastic fluid. For simplicity, we use the Oldroyd-B constitutive equation for solving $\boldsymbol{T}^p$ as follows:

$$\tau\left[\frac{\partial\boldsymbol{T}^p}{\partial t}+\boldsymbol{u}\cdot\boldsymbol{\nabla}\boldsymbol{T}^p-(\boldsymbol{T}^p\cdot\boldsymbol{\nabla}\boldsymbol{u}+\boldsymbol{\nabla}\boldsymbol{u}^{\mathrm{T}}\cdot\boldsymbol{T}^p)\right]+\boldsymbol{T}^p=\mu^p(\boldsymbol{\nabla}\boldsymbol{u}+\boldsymbol{\nabla}\boldsymbol{u}^{\mathrm{T}}), \tag{2.3}$$

where μ^p and τ are the polymeric viscosity (i.e. the non-Newtonian part) and the relaxation time of the viscoelastic fluid, respectively. The total viscosity of the viscoelastic fluid is the sum of the solvent viscosity and the polymeric viscosity, i.e. $\mu=\mu^s+\mu^p$. Note that the viscoelasticity of only the internal fluid is considered in the present study, while the external fluid is Newtonian.

The capsule membrane is considered as an infinitely thin interface with resistances against shear deformation, area dilatation and bending. For the former two resistances, we use the Skalak (SK) constitutive law (Skalak *et al.* 1973), in which the strain energy function is:

$$W_e=\frac{E_s}{4}(\lambda_1^4+\lambda_2^4-2\lambda_1^2-2\lambda_2^2+2)+\frac{E_a}{4}(\lambda_1^2\lambda_2^2-1)^2. \tag{2.4}$$

https://doi.org/10.1017/jfm.2018.88 Published online by Cambridge University Press

Here, λ_1 and λ_2 ($\lambda_1 \geqslant \lambda_2$) are the principal in-plane stretch ratios, and E_s and E_a are the moduli of shear and area dilatation. Accordingly, the principal stresses τ_1 and τ_2 ($\tau_1 \geqslant \tau_2$) in the capsule membrane can be calculated:

$$\tau_1 = E_s \frac{\lambda_1}{\lambda_2}(\lambda_1^2 - 1) + E_a \lambda_1 \lambda_2 (\lambda_1^2 \lambda_2^2 - 1), \tag{2.5}$$

$$\tau_2 = E_s \frac{\lambda_2}{\lambda_1}(\lambda_2^2 - 1) + E_a \lambda_1 \lambda_2 (\lambda_1^2 \lambda_2^2 - 1). \tag{2.6}$$

The resistance against bending is modelled by using the Helfrich bending energy function (Helfrich 1973) as follows:

$$W_b = \frac{E_b}{2} \int_S (2H - C_0)^2 \, \mathrm{d}S, \tag{2.7}$$

where E_b is the bending modulus, and H and C_0 are the mean and spontaneous curvatures, respectively. The forces resulting from the bending resistance can then be calculated:

$$\boldsymbol{f}_b = -E_b[(2H - C_0)(2H^2 - 2\kappa_g + C_0 H) + 2\Delta_s H]\boldsymbol{n}, \tag{2.8}$$

where κ_g is the Gaussian curvature, $\boldsymbol{n}$ is the outward unit normal vector and Δ_s is the Laplace–Beltrami operator. In the present study, we pay particular attention to the effects of the internal fluid viscoelasticity on the dynamics of the whole capsule. Therefore, the above-described constitutive laws (i.e. the SK constitutive law and the Helfrich bending energy function) for membrane mechanics are employed in all the following simulations, which have been widely used for biological membranes and some artificial capsules (Barthes-Biesel 2016). Nevertheless, other constitutive laws can be easily implemented in the future, when our present numerical model is used for analysing any specific examples of viscoelastic capsules, for example, white blood cells or artificial capsules enclosing macromolecules or gel cores.

2.2. *Front-tracking method*

The two-phase flow system (i.e. the flows inside and outside the capsule) is solved using the front-tracking finite-difference method, which is firstly proposed by Unverdi & Tryggvason (1992) for incompressible multi-fluid flows. Based on this method, we recently developed a three-dimensional model for simulating the deformation and dynamics of capsules enclosing a Newtonian fluid (hereafter referred to as Newtonian capsules). In our model, a finite-element method is integrated for the computation of the elastic stress in the capsule membrane (Luo *et al.* 2013, 2015). Here, we only outline this model briefly and especially emphasize the essential changes as it is applied to the study of the flow dynamics of viscoelastic capsules. Nevertheless, more details can be found in the referenced studies (Li & Sarkar 2008; Yazdani & Bagchi 2012; Luo *et al.* 2013, 2015).

In the front-tracking method, the viscoelastic fluid inside the capsule and the surrounding Newtonian fluid are treated as a single-phase fluid with sharp variations in material properties across the capsule membrane, such as density, solvent viscosity, polymeric viscosity and relaxation time. The flows inside and outside the capsule can then be obtained simultaneously on a stationary Eulerian grid by solving a single set of the flow-governing equations (i.e. (2.1) and (2.2)) in the whole

https://doi.org/10.1017/jfm.2018.88 Published online by Cambridge University Press

computational domain. Similarly, the viscoelastic constitutive equation (i.e. (2.3)) for the viscoelastic stress is also solved in the whole computational domain, while μ^p and τ are set to 0 outside the capsule since no viscoelastic stress is considered for the surrounding fluid in this study. This numerical treatment of the viscoelastic constitutive equation has been used in previous studies on viscoelastic drops (Aggarwal & Sarkar 2007; Izbassarov & Muradoglu 2015, 2016). For the convenience of implementation, all the material properties sharply varying across the membrane are constructed using an indicator function $I(\boldsymbol{x})$ that is 1 inside the capsule and 0 outside:

$$\phi(\boldsymbol{x}) = \phi_{out} + (\phi_{in} - \phi_{out})I(\boldsymbol{x}). \tag{2.9}$$

Here, ϕ represents the material properties (i.e. ρ, μ^s, μ^p and τ), and their corresponding values inside and outside the capsule are indicated by the subscripts 'in' and 'out', respectively. Since we only consider the internal fluid viscoelasticity in the present study, both μ^p_{out} and τ_{out} are set to 0 for the exterior of the capsule. To avoid the numerical instability owing to the sharp variations of the material properties, we define the indicator function $I(\boldsymbol{x})$ that is transformed to vary smoothly over a few Eulerian grid points across the membrane. The distribution of $I(\boldsymbol{x})$ is obtained by solving a Poisson equation based on the discrete form of the delta function (Unverdi & Tryggvason 1992; Tryggvason *et al.* 2001).

The capsule membrane is tracked by a set of non-stationary Lagrangian points, which are advected as follows:

$$\frac{\mathrm{d}\boldsymbol{x}'}{\mathrm{d}t} = \boldsymbol{u}'(\boldsymbol{x}'). \tag{2.10}$$

The velocity $\boldsymbol{u}'$ of Lagrangian points is interpolated from the velocity $\boldsymbol{u}$ of adjacent Eulerian grid points based on the delta function δ (Unverdi & Tryggvason 1992; Tryggvason *et al.* 2001):

$$\boldsymbol{u}'(\boldsymbol{x}') = \delta(x - x')\delta(y - y')\delta(z - z')\boldsymbol{u}(\boldsymbol{x}), \tag{2.11}$$

$$\delta(x - x') = \begin{cases} \dfrac{1}{4h_e}\left[1 + \cos\left(\pi\dfrac{x - x'}{2h_e}\right)\right] & \text{for } |x - x'| \leqslant 2h_e, \\ 0 & \text{for } |x - x'| > 2h_e. \end{cases} \tag{2.12}$$

Here, h_e is the Eulerian grid size. By connecting the Lagrangian points, the capsule membrane is approximated by an assembly of flat triangular plates. Thus, the large-deformation finite-element method proposed by Shrivastava & Tang (1993) can be employed to solve the elastic stress in the deformed membrane via the constitutive laws (e.g. (2.4)–(2.8)). More details about the solution of the strain and stress fields in the membrane can be found in the referenced studies (Li & Sarkar 2008; Yazdani & Bagchi 2012; Luo *et al.* 2013, 2015). In the front-tracking method, the elastic stress in the capsule membrane is transformed into a singular body force in the momentum equation, i.e. $\boldsymbol{f}$ on the right-hand side of (2.2). Notably, the membrane stress stored at the Lagrangian points is also distributed smoothly onto several adjacent Eulerian grid points via the delta distribution function δ to avoid numerical instability.

2.3. *Flow solver*

The governing equations are recast into the dimensionless form through scaling length by the capsule radius R, time by γ^{-1}, velocity by γR, pressure and viscoelastic stress

https://doi.org/10.1017/jfm.2018.88 Published online by Cambridge University Press

by $\rho_{out}\gamma^2R^2$ and membrane tension by $\mu_{out}\gamma$, where ρ_{out} and μ_{out} are the density and viscosity of the surrounding fluid, respectively. In the present study, the dynamics of a viscoelastic capsule freely suspended in a Newtonian fluid is considered. Therefore, the dimensionless parameters include the Reynolds number Re, the capillary number Ca, the Deborah number De, the density ratio λ_ρ, the ratio of the internal to the external total viscosity λ_μ, the ratio of the polymeric to the total viscosity β for the internal fluid, the ratio of the area dilatation to the shear modulus C and the ratio of the bending to the shear modulus E_b^*, which are defined respectively as follows:

$$\left.\begin{aligned} Re=\frac{\rho_{out}\gamma R^2}{\mu_{out}}, \quad Ca=\frac{\mu_{out}\gamma R}{E_s}, \quad De=\gamma\tau, \quad \lambda_\rho=\frac{\rho_{in}}{\rho_{out}}, \\ \lambda_\mu=\frac{\mu_{in}}{\mu_{out}}, \quad \beta=\frac{\mu_{in}^p}{\mu_{in}}, \quad C=\frac{E_a}{E_s}, \quad E_b^*=\frac{E_b}{R^2E_s}. \end{aligned}\right\} \tag{2.13}$$

Here, the subscripts '*in*' and '*out*' indicate the inside and outside of the capsule, respectively; the total viscosity is the sum of the solvent viscosity and the polymeric viscosity, i.e. $\mu_{in}=\mu_{in}^s+\mu_{in}^p$ and $\mu_{out}=\mu_{out}^s+\mu_{out}^p$, while μ_{out}^p is set to 0. Besides, De and β are both set to 0 for the external Newtonian fluid, and hence they are parameters for the internal viscoelastic fluid with omission of the subscript '*in*'. For simplicity, λ_ρ, C and E_b^* are set to 1, 1 and 0.01, which have been used in previous studies on Newtonian capsules (Kwak & Pozrikidis 2001; Pozrikidis 2001; Zhao & Bagchi 2011; Yazdani & Bagchi 2013; Luo & Bai 2016). Since our present numerical method (described in detail later) cannot simulate a Stokes flow (i.e. $Re=0$), we fix $Re=0.1$ to represent a low Reynolds number case (Aggarwal & Sarkar 2007; Bai *et al.* 2013; Luo *et al.* 2013). In our previous work (Luo *et al.* 2015), it has been indicated that $Re=0.1$ is sufficiently low to neglect the inertial effect on the dynamics of Newtonian capsules. Here, we further verify that little change is observed in both the transient and steady-state deformation of viscoelastic capsules with Re decreasing from 0.1 to 0.02; specifically, the largest relative change is below 1%. In this study, we focus on the effects of the internal fluid viscoelasticity. Thus the effects of varying De and β on the shape deformation and orientation dynamics of viscoelastic capsules with different Ca and λ_μ are systematically investigated. The capsule dynamics is characterized by Taylor parameters (Taylor 1934): (i) the deformation index, $D=(L-B)/(L+B)$, where L and B are the semimajor and semiminor axes of the capsule, respectively; and (ii) the orientation angle θ between the major axis and the flow direction. The two parameters D and θ are computed from the principal directions of the inertia tensor of the capsule shape (Ramanujan & Pozrikidis 1998).

The non-dimensionalized governing equations are solved using a fully three-dimensional finite-difference code on a regular collocated uniform Cartesian grid, in which the fluid velocity, material properties, pressure and viscoelastic stress are all located at the cell centre. Hence, the spatial derivatives can be discretized by using standard central-difference schemes. For the temporal discretization, the three-stage RKCN (Runge–Kutta/Crank–Nicholson) four-step projection method proposed by Ni, Komori & Morley (2003) is used to decouple the solution of pressure and velocity, in which the three-stage Runge–Kutta technique and the Crank–Nicolson semi-implicit technique are used to update the convective and diffusion terms, respectively. The Poisson equation for pressure is solved only in the last Runge–Kutta stage to reduce computational cost. As a result, this RKCN projection method can be expressed as follows:

https://doi.org/10.1017/jfm.2018.88 Published online by Cambridge University Press

$$A^m \boldsymbol{u}^{*m} = \boldsymbol{r}^m - (\alpha^m + \beta^m)\nabla p^n, \quad m = 1, 2, 3, \tag{2.14}$$

$$\boldsymbol{u}^{**m} = \boldsymbol{u}^{*m} + \Delta t(\alpha^m + \beta^m)\nabla p^n, \quad m = 1, 2, 3, \tag{2.15}$$

$$\boldsymbol{u}^m = \boldsymbol{u}^{**m} - \Delta t(\alpha^m + \beta^m)\sum_{l=1}^{3}(\alpha^l + \beta^l)\nabla p^n, \quad m = 1, 2, \tag{2.16}$$

$$\nabla \cdot \left[\sum_{l=1}^{3}(\alpha^l + \beta^l)\nabla p^{n+1}\right] = \frac{1}{\Delta t}\nabla \cdot \boldsymbol{u}^{**m}, \quad m = 3, \tag{2.17}$$

$$\boldsymbol{u}^m = \boldsymbol{u}^{**m} - \Delta t\sum_{l=1}^{3}(\alpha^l + \beta^l)\nabla p^{n+1}, \quad m = 3, \tag{2.18}$$

with

$$A^m = \frac{1}{\Delta t}\left[1 - \frac{\gamma^m \Delta t}{Re}\nabla \cdot (\mu^{s,n+1/2}\nabla)\right], \tag{2.19}$$

$$\begin{aligned}\boldsymbol{r}^m \;=\; & \frac{1}{\Delta t}\left[1 + \frac{\gamma^m \Delta t}{Re}\nabla \cdot (\mu^{s,n+1/2}\nabla)\right]\boldsymbol{u}^{m-1} \\ & + [\alpha^m(\boldsymbol{f} - \boldsymbol{u}\nabla\boldsymbol{u} + \nabla \cdot \boldsymbol{T}^p)^{m-1} + \beta^m(\boldsymbol{f} - \boldsymbol{u}\nabla\boldsymbol{u} + \nabla \cdot \boldsymbol{T}^p)^{m-2}],\end{aligned} \tag{2.20}$$

$$\frac{1}{\mu^{s,n+1/2}} = \frac{1}{2}\left(\frac{1}{\mu^{s,n}} + \frac{1}{\mu^{s,n+1}}\right), \tag{2.21}$$

$$\alpha^m = \left[\frac{8}{15}, \frac{5}{12}, \frac{3}{4}\right], \quad \beta^m = \left[0, -\frac{17}{60}, -\frac{5}{12}\right], \quad \gamma^m = \left[\frac{4}{15}, \frac{1}{15}, \frac{1}{6}\right]. \tag{2.22a–c}$$

Here, Δt is the time step size; m and n represent the Runge–Kutta stage number and the time step number, respectively. All the variables presented here are in the dimensionless form. Note that the superscripts '$m-1$' and '$m-2$' in (2.20) can be 0 and -1 at the first sub-step. The terms with -1 are ignored, and the terms with 0 have their corresponding values at the time step n. The positions of the Lagrangian points on the capsule membrane are updated in each Runge–Kutta stage as follows:

$$\boldsymbol{x}'^m = \boldsymbol{x}'^{m-1} + \Delta t(\alpha^m \boldsymbol{u}'^m + \beta^m \boldsymbol{u}'^{m-1}). \tag{2.23}$$

The elastic stress in the membrane is also solved in each Runge–Kutta stage according to the updated positions of the Lagrangian points.

It is required to invert a large matrix to obtain the intermediate velocity $\boldsymbol{u}^{*m}$ by solving (2.14):

$$\begin{aligned}&\left\{1 - \frac{\gamma^m \Delta t}{Re}\left[\frac{\partial}{\partial x}\left(\mu^{s,n+1/2}\frac{\partial}{\partial x}\right) + \frac{\partial}{\partial y}\left(\mu^{s,n+1/2}\frac{\partial}{\partial y}\right) + \frac{\partial}{\partial z}\left(\mu^{s,n+1/2}\frac{\partial}{\partial z}\right)\right]\right\}\boldsymbol{u}^{*m} \\ &\quad = \Delta t[\boldsymbol{r}^m - (\alpha^m + \beta^m)\nabla p^n].\end{aligned} \tag{2.24}$$

To improve the efficiency of the numerical method, we employ the approximate factorization technique (Zang, Street & Koseff 1994; Chinyoka *et al.* 2005), in which (2.24) can be rewritten as:

$$\left[1 - \frac{\gamma^m \Delta t}{Re}\frac{\partial}{\partial x}\left(\mu^{s,n+1/2}\frac{\partial}{\partial x}\right)\right]\left[1 - \frac{\gamma^m \Delta t}{Re}\frac{\partial}{\partial y}\left(\mu^{s,n+1/2}\frac{\partial}{\partial y}\right)\right]$$

https://doi.org/10.1017/jfm.2018.88 Published online by Cambridge University Press

$$\times \left[1 - \frac{\gamma^m \Delta t}{Re}\frac{\partial}{\partial z}\left(\mu^{s,n+1/2}\frac{\partial}{\partial z}\right)\right]\boldsymbol{u}^{*m} = \Delta t[\boldsymbol{r}^m - (\alpha^m + \beta^m)\nabla p^n]. \tag{2.25}$$

Alternatively, the inversion of (2.25) requires solving three tridiagonal matrices, which significantly reduces the computing time and the memory requirements.

Notably, since in projection methods the solution of the pressure Poisson equation (i.e. (2.17)) consumes most of the computing time, in our present method the pressure Poisson equation is solved only in the last Runge–Kutta stage to save computing time. Besides, the four-level multigrid technique and the alternating-direction implicit scheme are used to solve the discretized pressure Poisson equation to accelerate the convergence.

2.4. *Solution of the viscoelastic constitutive equation*

In previous studies on viscoelastic drops using the front-tracking method (Aggarwal & Sarkar 2007; Izbassarov & Muradoglu 2015, 2016), the convection term of the viscoelastic constitutive equation (i.e. (2.3)) is treated explicitly. As a result, special treatments are needed to simulate viscoelastic flows with high Deborah numbers, such as the semi-analytical method and the log-conformation method (Fattal & Kupferman 2005; Aggarwal & Sarkar 2007; Izbassarov & Muradoglu 2015). In our study, the convection term in (2.3) is treated implicitly (Chinyoka *et al.* 2005), while other terms are explicitly treated as follows:

$$De\left[\frac{(\boldsymbol{T}^p)^{n+1} - (\boldsymbol{T}^p)^n}{\Delta t} + \boldsymbol{u}^n \cdot (\nabla \boldsymbol{T}^p)^{n+1} - (\boldsymbol{T}^p \cdot \nabla \boldsymbol{u} + \nabla \boldsymbol{u}^{\mathrm{T}} \cdot \boldsymbol{T}^p)^n\right] + (\boldsymbol{T}^p)^{n+1} = \left[\frac{\mu^p}{Re}(\nabla \boldsymbol{u} + \nabla \boldsymbol{u}^{\mathrm{T}})\right]^n. \tag{2.26}$$

Note that all the variables presented here are in dimensionless form. The effect of the viscoelastic stress on the flow field is included explicitly into the three-stage RKCN four-step projection method as shown in (2.14) and (2.20). The viscoelastic stress needs to be updated in each Runge–Kutta stage owing to the update of the fluid velocity. Thus, the viscoelastic constitutive equation (i.e. (2.3)) is also solved in each Runge–Kutta stage, where the effective time step size is $\Delta t' = (\alpha^m + \beta^m)\Delta t$. Then, equation (2.26) is transformed to:

$$\left[1 + \frac{De \cdot \Delta t'}{De + \Delta t'}\left(u^{m-1}\frac{\partial}{\partial x} + v^{m-1}\frac{\partial}{\partial y} + w^{m-1}\frac{\partial}{\partial z}\right)\right]\boldsymbol{T}^{p,m} = \frac{\Delta t'}{De + \Delta t'}\left[\frac{\mu^p}{Re}(\nabla u + \nabla u^{\mathrm{T}}) + De(\boldsymbol{T}^p \cdot \nabla u + \nabla u^{\mathrm{T}} \cdot \boldsymbol{T}^p) + \frac{De}{\Delta t'}\boldsymbol{T}^p\right]^{m-1}. \tag{2.27}$$

Here, u, v and w are the three components of the fluid velocity vector $\boldsymbol{u}$. In analogy to the solution of the momentum equation (i.e. (2.24)), the above viscoelastic constitutive equation (i.e. (2.27)) is also factorized:

$$\left(1 + \frac{De \cdot \Delta t'}{De + \Delta t'}u^{m-1}\frac{\partial}{\partial x}\right)\left(1 + \frac{De \cdot \Delta t'}{De + \Delta t'}v^{m-1}\frac{\partial}{\partial y}\right)\left(1 + \frac{De \cdot \Delta t'}{De + \Delta t'}w^{m-1}\frac{\partial}{\partial z}\right)\boldsymbol{T}^{p,m} = \frac{\Delta t'}{De + \Delta t'}\left[\frac{\mu^p}{Re}(\nabla \boldsymbol{u} + \nabla \boldsymbol{u}^{\mathrm{T}}) + De(\boldsymbol{T}^p \cdot \nabla \boldsymbol{u} + \nabla \boldsymbol{u}^{\mathrm{T}} \cdot \boldsymbol{T}^p) + \frac{De}{\Delta t'}\boldsymbol{T}^p\right]^{m-1}. \tag{2.28}$$

https://doi.org/10.1017/jfm.2018.88 Published online by Cambridge University Press

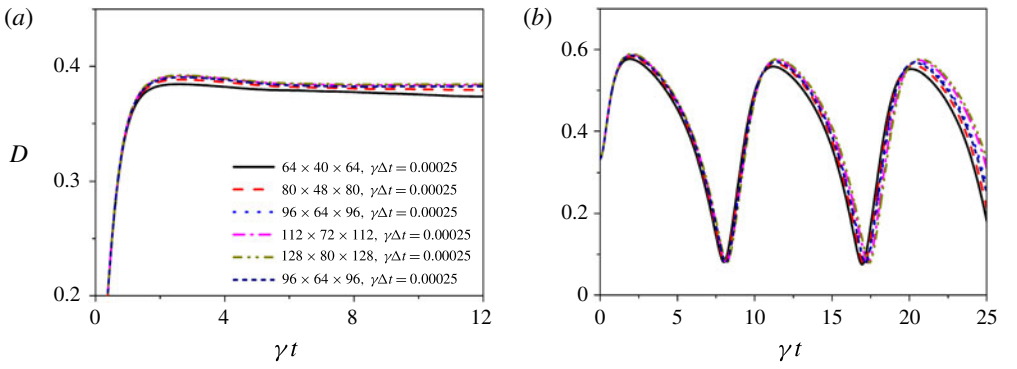


FIGURE 2. (Colour online) Convergence study of the deformation D plotted against the dimensionless time γt with varying Eulerian grid resolution at $Ca = 0.5$, $De = 1.0$, $\lambda_\mu = 1.0$ and $\beta = 0.5$. (*a*) An initially spherical capsule. (*b*) An initially non-spherical capsule with aspect ratio $a/b = 2$.

Thus, the solution of the viscoelastic constitutive equation can be realized efficiently by solving three tridiagonal matrices. Spatially, the standard central-difference scheme is employed.

3. Results and discussion

3.1. *Convergence study and model validation*

To justify the accuracy of our numerical method, we first conduct a convergence test. In general, the effects of the computational domain size, the time step size and the Eulerian and Lagrangian resolutions need to be examined. Our previous study on Newtonian capsules (Luo *et al.* 2015) shows that a computational domain size of $L_x \times L_y \times L_z = 8R \times 5R \times 8R$ and a Lagrangian resolution of 5120 triangular elements are sufficient to eliminate their effects, which is therefore used in the present study. Owing to the presence of the internal fluid viscoelasticity, we need to reexamine the effects of the Eulerian resolution and the time step size. As presented in figure 2, the time evolution of the deformation index D is plotted for an initially spherical capsule and an ellipsoidal capsule at $Ca = 0.5$, $De = 1.0$, $\lambda_\mu = 1.0$ and $\beta = 0.5$ with varying Eulerian resolution and time step size. The Eulerian discretization level increases from $64 \times 40 \times 64$ up to a maximum of $128 \times 80 \times 128$ and the time step size decreases from 2.5×10^{-4} to a minimum of 5×10^{-5}. As the Eulerian resolution or the time step size increases, a slight increase in D is observed for both the spherical and ellipsoidal capsules. We use a grid of $96 \times 64 \times 96$ for the following simulations since D presents insignificant changes from that at a grid of $128 \times 80 \times 128$, e.g. only 0.4 % for the equilibrium deformation D_{st} of the spherical capsule and 1 % for the maximum deformation D_{max} of the ellipsoidal capsule. Regarding the time step size, $\Delta t = 2.5 \times 10^{-4}$ is used, as the variation in both D_{st} and D_{max} is below 1 % when Δt decreases to 5×10^{-5}. Besides, we are convinced by that comparable values of the Eulerian resolution and the time step size have also been used in previous studies on the deformation and breakup of viscoelastic drops (Aggarwal & Sarkar 2007).

We next present the validation of our model by comparing with reported data from previous studies in figure 3. Note that we validate the membrane elasticity model and the internal fluid viscoelasticity model separately, as no data are available for

https://doi.org/10.1017/jfm.2018.88 Published online by Cambridge University Press

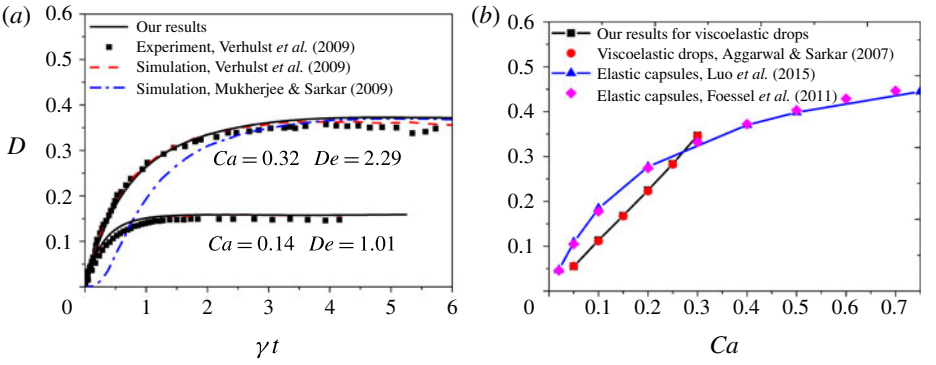


FIGURE 3. (Colour online) Model validation. (*a*) The transient deformation of viscoelastic drops (i.e. a viscoelastic fluid surrounded by a clean interface having uniform surface tension) with $\lambda_\mu = 1.5$ and $\beta = 0.32$. (*b*) The equilibrium deformation of viscoelastic drops with $De = 0.5$, $\lambda_\mu = 1$ and $\beta = 0.5$. Results for Newtonian capsules (i.e. a Newtonian fluid surrounded by an elastic membrane) with $\lambda_\mu = 1.0$ from our previous work are also presented for comparison purposes.

viscoelastic capsules to the best of our knowledge. In our previous work (Luo *et al.* 2015), the membrane elasticity model is validated by simulating the deformation of Newtonian capsules in simple shear flow and comparing with other methods, e.g. the boundary integral method by Foessel *et al.* (2011). Here, the validation data are included in figure 3(*b*) for comparison purposes. The only difference of viscoelastic capsules from Newtonian capsules is the presence of viscoelasticity in the internal fluid. Thus we further validate the solution of the viscoelastic constitutive equation in the present study. This validation is realized by simulating the deformation of a viscoelastic drop in simple shear flow which consists of a viscoelastic fluid enclosed by a clean interface with uniform interfacial tension. As shown in figure 3, quantitative comparisons between our method and those of others, including the volume-of-fluid method and experiments by Verhulst *et al.* (2009*b*) and the front-tracking method by Sarkar *et al.* (Aggarwal & Sarkar 2007; Mukherjee & Sarkar 2009), are conducted by predicting both the transient and equilibrium deformations of the viscoelastic drop. With the same initial flow condition (i.e. a quiescent fluid with impulsively started walls), a relatively large difference is observed in the initial stage of the transient deformation between Sarkar's results (Mukherjee & Sarkar 2009) and those by Verhulst *et al.* (Verhulst *et al.* 2009*b*). In Sarkar's study (Mukherjee & Sarkar 2009), this difference is attributed to finite inertia resulting in a delayed development of the shear flow (i.e. $Re = 0.1$ in Sarkar's paper is higher than $Re = 0.01$–0.05 in Verhulst's study). It is indicated by that the result of the same viscoelastic drop deforming under a different initial flow condition (i.e. fully developed shear) matches Verhulst's experimental observation very well. Therefore, the fully developed shear flow is used as the initial flow condition in our present validation. Our results of the transient drop deformation are also very similar to those from both the volume-of-fluid method and experiments by Verhulst *et al.* (2009*b*), e.g. the largest differences are only 3.5 % and 6.5 % respectively. Besides, excellent agreement is observed in the prediction of the steady-state value of the drop deformation between our results and those from the front-tracking method by Sarkar *et al.* (Aggarwal & Sarkar 2007; Mukherjee & Sarkar 2009); for instance, the deviation is below 1.5 %. These comparisons indicate the acceptably high accuracy of our numerical method.

https://doi.org/10.1017/jfm.2018.88 Published online by Cambridge University Press

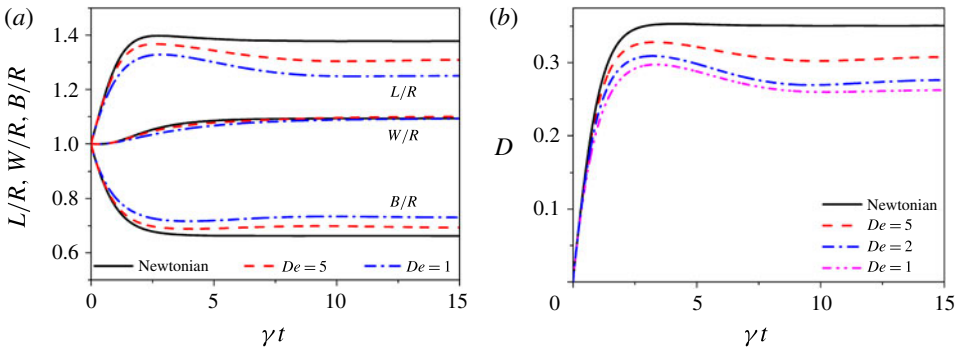


FIGURE 4. (Colour online) Effects of the internal fluid viscoelasticity on the transient deformation of capsules with $Ca = 0.5$, $\lambda_\mu = 5$ and $\beta = 0.5$. The Deborah number De is varied. The Newtonian case with $Ca = 0.5$ and $\lambda_\mu = 2.5$ is also plotted for the comparison purpose. (*a*) Time evolutions of the semimajor axis L, the semiminor axis B and the half-axis length W in the vorticity direction. (*b*) Time evolution of the deformation index D.

3.2. *Deformation of spherical viscoelastic capsules*

In this section, we examine the effects of the internal fluid viscoelasticity (i.e. varying the Deborah number De and the ratio of the polymeric to the total viscosity β) on the deformation behaviours of initially spherical capsules with different capillary numbers Ca and viscosity ratios λ_μ. The transient deformation is first presented at different De and compared with that of Newtonian capsules. In general, the deformation of spherical capsules always reaches a steady state eventually, in which either the shape or the orientation of the whole capsule remains unchanged over time. Consequently, the effects of De and β on the steady-state deformation and orientation are then studied. Next, we present a detailed discussion of the condition when the internal fluid viscoelasticity may have great effects on the capsule dynamics. Following this discussion, we present simulation results showing the effects of De and β under the condition that the internal fluid stress, particularly the internal viscoelastic stress, plays a predominant role in the determination of the capsule dynamics.

We first present the transient deformation of viscoelastic capsules. In figure 4, we plot the transient evolution of the lengths of the three principal axes (i.e. the semimajor axis L, the semiminor axis B and the half-axis length W in the vorticity direction) and the deformation index D for varying De at $Ca = 0.5$, $\lambda_\mu = 5$ and $\beta = 0.5$. The results of a Newtonian capsule with a total viscosity $\lambda_\mu = 2.5$ the same as the solvent viscosity (i.e. the Newtonian part) of the viscoelastic capsule are also presented in figure 4. For both the viscoelastic and Newtonian cases, the capsule elongates in L and W while it shortens in B; eventually, the capsule deformation reaches a steady state, in which L, W, B and hence the whole shape of the capsule present no change over time. Varying De induces changes in L and B with opposite tendencies and hence causes great variations in D, while it causes a very slight change in W, particularly for their steady-state values. Note that D increases monotonically to its steady-state value for the Newtonian capsule, while an overshoot is observed in the transient deformation of the viscoelastic capsule with the main contribution from the overshoot in L. This overshoot may be explained by the fact that the viscoelastic stress inhibiting capsule deformation needs a finite time to fully develop, corresponding to the relaxation time in the Oldroyd-B constitutive equation (see the

https://doi.org/10.1017/jfm.2018.88 Published online by Cambridge University Press

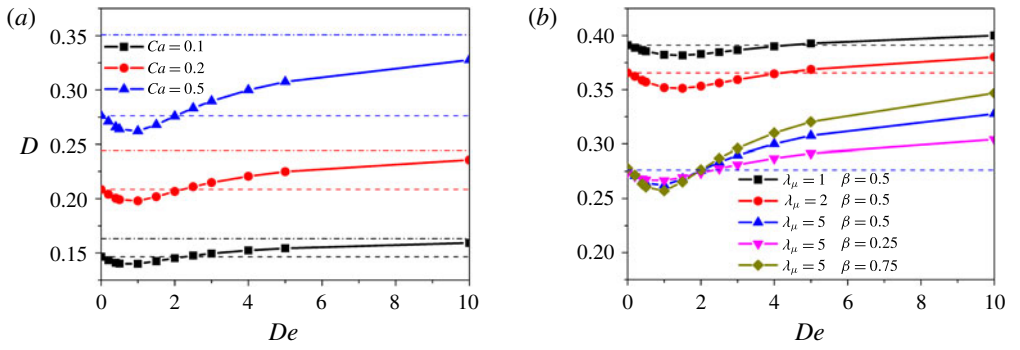


FIGURE 5. (Colour online) Effects of the internal fluid viscoelasticity on the steady-state deformation D of capsules. (*a*) D versus the Deborah number De at varying Ca at $\lambda_\mu = 5$ and $\beta = 0.5$. The dash and dash-dot lines indicate the deformation of purely Newtonian capsules with $\lambda_\mu = 5$ and 2.5, respectively. (*b*) Varying λ_μ and β at a fixed value of $Ca = 0.5$. The steady-state values of the capsule deformation are obtained at $\gamma t = 15$.

discussion in § 3.3). Particularly, the time scales of the capsule deformation and the viscoelastic stress development are characterized by Ca and De, respectively. As reported by Yue *et al.* (2005*a*) for viscoelastic drops, when $De/Ca > 1$–5, the viscoelastic stress develops too slowly to keep up with the varying strain rate from the deforming drop shape and overshoot may present in the drop deformation as a consequence. Note that the critical value of De/Ca strongly depends on several other factors, for example, the viscosity ratio.

Next, we study the effects of the internal fluid viscoelasticity on the steady-state deformation of viscoelastic capsules. For this purpose, the steady-state deformation index D is plotted in figure 5 as a function of De at varying Ca and λ_μ. As expected, at each given value of De and β, D increases with increasing Ca or decreasing λ_μ, and it is consistent with the observation for Newtonian capsules (Lac *et al.* 2004; Foessel *et al.* 2011; Barthes-Biesel 2016). However, we note that varying De or β also causes substantial effects in D. As De increases, D decreases first and then increases for all the cases of varying Ca, λ_μ and β. As seen in (2.2) and (2.3), $De = 0$ is equivalent to the Newtonian case with a viscosity ratio of $(\mu^s_{in} + \mu^p_{in})/\mu_{out}$. When De increases from 0 to around $O(1)$, the rapidly developed viscoelastic stress inhibits capsule deformation (the underlying mechanism is discussed in § 3.3), but the reduction in D is generally slight (less than 10 %). A similar phenomenon is observed for viscoelastic drops in previous numerical studies (Yue *et al.* 2005*b*; Aggarwal & Sarkar 2007) which are, however, limited to low De (i.e. around $O(1)$). In figure 5, we find that when De further increases to be much higher than $O(1)$ (e.g. around $O(10)$), D shows an increasing tendency in contrast and gradually approaches that of another Newtonian case with a viscosity ratio of μ^s_{in}/μ_{out}. In fact, the viscoelastic stress is expected to be negligible when De becomes infinite, and hence $De \sim \infty$ should be just equivalent to the Newtonian case of μ^s_{in}/μ_{out}. Note that the reduction extent of the capsule deformation in the decreasing stage, i.e. De increasing from 0 to around $O(1)$, is generally much smaller than the increasing extent in the increasing stage, i.e. De increasing from around $O(1)$ to infinite. Figure 5(*b*) presents the effects of β on the steady-state deformation. At low De when the internal viscoelastic stress inhibits capsule deformation, D decreases with β because increasing β is equivalent to enlarging the contribution of the viscoelastic stress and hence enhances its suppressing

https://doi.org/10.1017/jfm.2018.88 Published online by Cambridge University Press

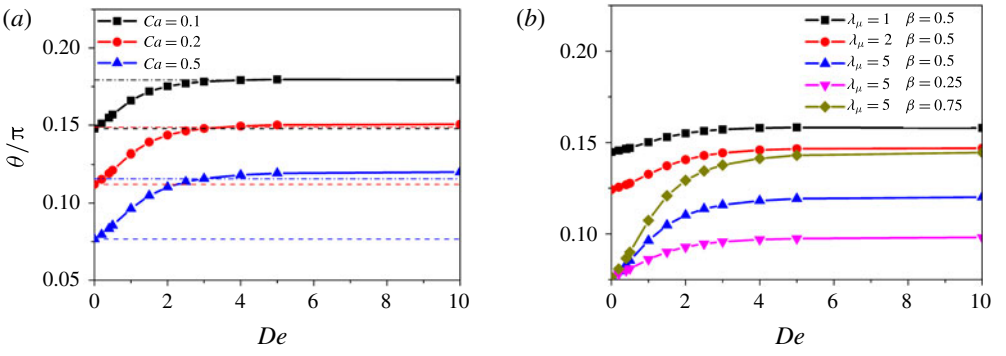


FIGURE 6. (Colour online) Effects of the internal fluid viscoelasticity on the steady-state orientation of capsules. Same parameter values are used as in figure 5.

effect. In contrast, D increases with β at high De when the internal viscoelastic stress makes a much lower contribution to the capsule deformation. Under this circumstance, the capsule deformation is largely dependent on the solvent viscosity $(1-\beta)\lambda_\mu$ (i.e. the Newtonian part of the internal viscoelastic fluid), and in general, it decreases significantly with λ_μ for Newtonian cases (Foessel *et al.* 2011; Barthes-Biesel 2016).

In figure 6, the steady-state orientation angle θ is plotted as a function of De for varying Ca and λ_μ. The orientation θ decreases with Ca or λ_μ as expected, which is consistent with the case of Newtonian capsules (Lac *et al.* 2004; Foessel *et al.* 2011; Barthes-Biesel 2016). For all the cases of viscoelastic capsules with varying Ca, λ_μ and β, as De increases from 0, θ monotonically increases from that of the Newtonian limit of $(\mu^s_{in}+\mu^p_{in})/\mu_{out}$ with an obvious degree at low De. As De increases to higher values, θ increases gradually and eventually reaches a plateau value which is very close to that of another Newtonian limit of μ^s_{in}/μ_{out}. Besides, θ is observed to increase with increasing β which indicates the decrease of the internal solvent viscosity, because the capsule orientation decreases with the internal viscosity (Foessel *et al.* 2011). These results demonstrate that the orientation dynamics of the capsules is also significantly affected by the internal fluid viscoelasticity.

Next, we discuss the condition when the internal fluid viscoelasticity may have significant effects on the capsule dynamics. The capsule dynamics is governed by the competitive relation between the elastic load $\boldsymbol{f_e}$ from the membrane stress and the jump in the fluid stress $\boldsymbol{T}$ across the capsule membrane (Barthes-Biesel & Rallison 1981; Foessel *et al.* 2011; Barthes-Biesel 2016):

$$\boldsymbol{T}_{out}\cdot\boldsymbol{n}-\boldsymbol{T}_{in}\cdot\boldsymbol{n}=\frac{1}{Ca}\boldsymbol{f}_e. \tag{3.1}$$

Here, $\boldsymbol{n}$ is the outward unit normal vector; $\boldsymbol{T}_{out}$ and $\boldsymbol{T}_{in}$ are the fluid stresses at the capsule membrane from the external and internal flows, respectively. Since the viscoelastic stress is considered only in the internal fluid and the no-slip boundary condition is applied at the capsule membrane, $\boldsymbol{T}_{out}$ and $\boldsymbol{T}_{in}$ can be given in the non-dimensional form as follows:

$$\boldsymbol{T}_{out}=-p\boldsymbol{I}+(\nabla\boldsymbol{u}+\nabla\boldsymbol{u}^{\mathrm{T}}), \tag{3.2}$$

$$\boldsymbol{T}_{in}=-p\boldsymbol{I}+\lambda_\mu[(1-\beta)(\nabla\boldsymbol{u}+\nabla\boldsymbol{u}^{\mathrm{T}})+\beta\boldsymbol{T}^p_{in}]. \tag{3.3}$$

https://doi.org/10.1017/jfm.2018.88 Published online by Cambridge University Press

As seen in (2.3) and (3.3), the effects of the internal fluid viscoelasticity, even the internal total viscosity including both Newtonian and non-Newtonian parts, vanish if the internal fluid is quiescent. Therefore, the internal fluid viscoelasticity has no influence on the steady-state deformation of capsules suspended in hyperbolic flow (or planar extensional flow), since the capsule membrane and the internal fluid become motionless at the steady state (Dodson & Dimitrakopoulos 2009; Barthes-Biesel 2016). For this reason, in the present study, we focus on the dynamics of viscoelastic capsules suspended in a simple shear flow, in which the fluid inside the capsule flows owing to the membrane rotation and hence the internal fluid viscoelasticity may have a strong impact on the capsule dynamics. As shown in (3.1), the membrane stress is dominating the capsule dynamics for $Ca \ll 1$ and hence the internal fluid viscoelasticity is expected to have negligible effects. From another perspective, the effects of the internal fluid viscoelasticity are justifiably supposed to be especially prominent at high Ca, which is obviously indicated in figure 5(*a*). The capillary number Ca is defined with the external fluid viscosity alone (see (2.13)), but the viscoelasticity is presented in the internal fluid. Therefore, together with Ca, the viscosity ratio λ_μ is another important parameter governing the impact extent of the internal fluid viscoelasticity on the capsule deformation, as shown in (3.2) and (3.3). For very low viscosity ratios (e.g. $\lambda_\mu < 0.2$), the internal fluid stress $\boldsymbol{T}_{in}$ has little effect on the capsule deformation (Foessel *et al.* 2011). Consequently, the effects of the internal fluid viscoelasticity tend to vanish at $\lambda_\mu \ll 1$ but it will become more prominent as λ_μ increases, which is consistent with the results presented in figure 5(*b*) In contrast, for large values of λ_μ, the internal fluid stress $\boldsymbol{T}_{in}$ is dominating the capsule deformation, as explored by Barthes-Biesel & Rallison (1981) who use the small-deformation analysis for Newtonian capsules. They suggest that for $\lambda_\mu \gg 1$ the capsule deformation exclusively depends on λ_μ alone as follows (Barthes-Biesel & Rallison 1981; Foessel *et al.* 2011):

$$D = \frac{5}{4\lambda_\mu} + O\left(\frac{1}{\lambda_\mu^2}, \frac{1}{Ca\lambda_\mu^2}\right). \tag{3.4}$$

As shown from the above analysis, especially (3.2) and (3.3), the viscoelastic stress of the internal fluid may have significant effects on the capsule deformation at large λ_μ, although it still strongly depends on β, measuring the contribution of the viscoelasticity to the internal fluid stress.

Then, we examine the effects of the internal fluid viscoelasticity on the capsule dynamics under the condition that the internal fluid stress, particularly the internal viscoelastic stress, plays a predominant role. To this end, we plot the characteristic parameters in figure 7, including the transient deformation, the steady-state deformation and orientation, and the tank-treading period, as functions of De at large λ_μ (i.e. $\lambda_\mu = 5$–20) with relatively high β (i.e. $(1-\beta)\lambda_\mu = 1$). In general, it is observed that the effects of De become greater as λ_μ increases. At large viscosity ratios (e.g. $\lambda_\mu = 15$), the transient deformation and orientation curves in figure 7(*a*) exhibit significant overshoots accompanied with decaying oscillations, which is also observed for Newtonian capsules (Ramanujan & Pozrikidis 1998). Note that these decaying oscillations are especially prominent at low Deborah numbers (e.g. $De = 0.1$), but they vanish at large De (e.g. $De = 10$). Due to the presence of these decaying oscillations, the capsules with lower De need a longer time to reach the steady state. As shown in figure 7(*b*), the steady-state value of D increases with De in general, although it shows a slight decrease at low De. When De becomes infinite, D for capsules with

https://doi.org/10.1017/jfm.2018.88 Published online by Cambridge University Press

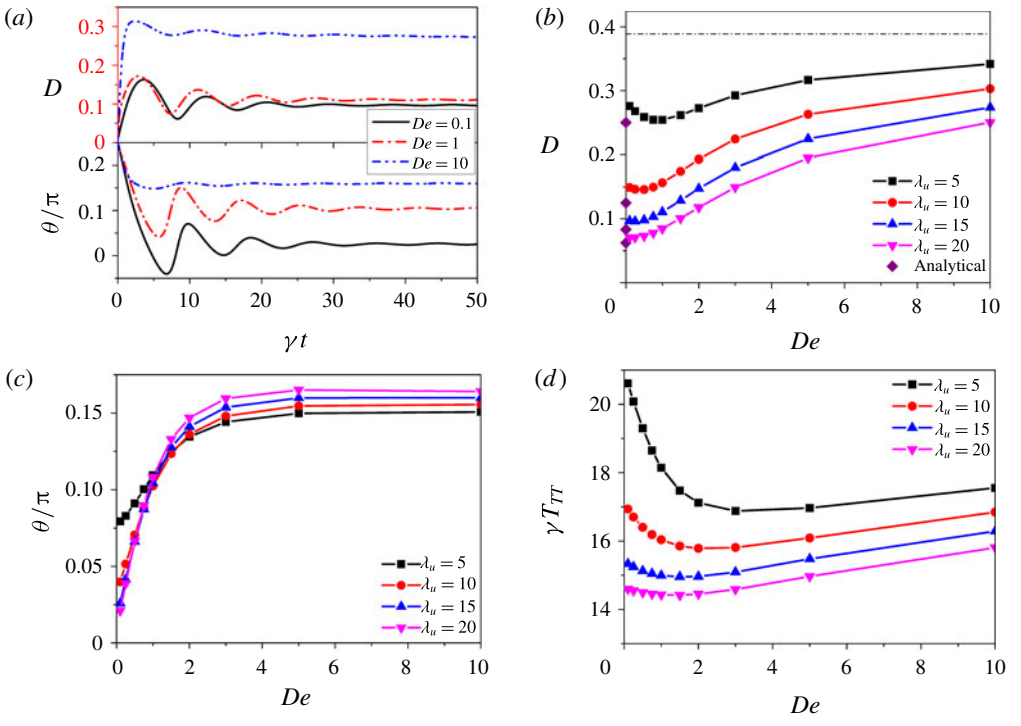


FIGURE 7. (Colour online) Effects of the internal fluid viscoelasticity on the capsule deformation at large viscosity ratios, i.e. $\lambda_\mu = 5$–20. Ca and μ^s_{in}/μ_{out} are fixed at 0.5 and 1, respectively. (*a*) Transient evolution of the deformation index and orientation angle for $\lambda_\mu = 15$. (*b*) The steady-state deformation index, (*c*) the steady-state orientation angle and (*d*) the tank-treading period versus the Deborah number De. The analytical prediction in (*b*) is calculated from (3.4) and the dash-dot line represents the corresponding value for the Newtonian case with $\lambda_\mu = 1$.

different λ_μ becomes close to the same upper limit, which is the Newtonian limit with the viscosity ratio of $\mu^s_{in}/\mu_{out} = 1$. On the other hand, when De approaches 0, D becomes close to the λ_μ-dependent lower limit, i.e. the Newtonian limit with the viscosity ratio of $\lambda_\mu = (\mu^s_{in} + \mu^p_{in})/\mu_{out}$. This is indicated by the good agreement between our numerical results for viscoelastic capsules with $De = 0.1$ and analytical results from the small-deformation theory for Newtonian capsules (3.4). Since the lower limit decreases with λ_μ while the upper limit remains the same, the effects of De on the deformation of viscoelastic capsules become greater at higher λ_μ. As shown in figure 7(*c*), the steady-state value of θ increases monotonically with De at all given values of λ_μ, and eventually reaches a plateau value. At very low De (e.g. $De = 0.1$), θ decreases significantly as λ_μ increases from 5 to 20, which is similar to that for Newtonian capsules (Foessel *et al.* 2011). In contrast, at large De (e.g. $De = 10$), θ increases slightly with λ_μ increasing. The underlying mechanism is discussed in the following section (i.e. § 3.3).

In our simulations, all viscoelastic capsules with initially spherical shape exhibit the tank-treading motion, which was previously demonstrated for Newtonian capsules (Barthes-Biesel 2011, 2016). In this mode, the capsule maintains a steady shape and orientation, while its membrane presents a continuous rotation. As shown in

https://doi.org/10.1017/jfm.2018.88 Published online by Cambridge University Press

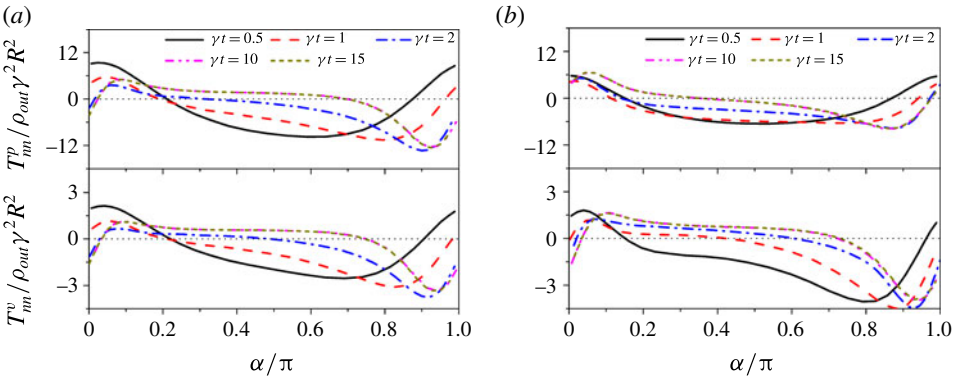


FIGURE 8. (Colour online) Time evolution of the normal viscous T^v and viscoelastic T^p stresses $T_{nn} = \boldsymbol{n} \cdot \boldsymbol{T} \cdot \boldsymbol{n}$, where $\boldsymbol{n}$ is the outward normal to the interface, along the inner edge of the capsule membrane for different Deborah numbers, i.e. $De = 0.1$ in (*a*) and $De = 1$ in (*b*). Here, $Ca = 0.5$, $\mu^s_{in}/\mu_{out} = 1$ and $\lambda_\mu = 5$. The normal stresses are plotted as functions of the phase angle α in the shear plane (i.e. $y = L_y/2$), which is defined as shown in the inset in figure 10(*d*).

figure 7(*d*), the Deborah number also has significant effects on the tank-treading period T_{TT}, i.e. the rotation period of the membrane. Note that T_{TT} is observed to decrease with the viscosity ratio λ_μ, which is contrary to that of Newtonian capsules predicted from the small-deformation theory by Keller & Skalak (1982). This inconsistency is due to the fact that large deformation of the whole capsule exerts substantial effects on the tank-treading motion which is heavily dependent on the viscosity ratio but neglected in the small-deformation theory. More importantly, we find that for each given value of λ_μ, as De increases continuously, T_{TT} decreases first and then increases, which is especially prominent at low λ_μ. These results indicate the significant effects of the internal fluid viscoelasticity on the tank-treading motion of spherical capsules.

3.3. *Analysis of fluid stresses*

In this section, we present a detailed analysis of the fluid stresses acting on the capsule membrane to further understand the mechanisms underlying the effects of the internal fluid viscoelasticity on the capsule dynamics (see figures 4–7). As shown in (3.1)–(3.3), the capsule deformation is determined by the fluid stresses $\boldsymbol{T}_{out}$ and $\boldsymbol{T}_{in}$ acting on the membrane from the external and internal flows, while the internal fluid viscoelasticity only makes a direct contribution to the internal fluid stress $\boldsymbol{T}_{in}$. Therefore, we mainly analyse the internal fluid stress $\boldsymbol{T}_{in}$ consisting of the viscous stress $\boldsymbol{T}^v$, the pressure p and the viscoelastic stress $\boldsymbol{T}^p$ (i.e. $\boldsymbol{T} = \boldsymbol{T}^v + \boldsymbol{T}^p - p\boldsymbol{I}$) and its dependence on the Deborah number; note that the subscript 'in' is omitted for simplicity. As shown in figures 8–11, the normal and tangential components of the three parts of the internal fluid stress (i.e. $\boldsymbol{T}^v$, p and $\boldsymbol{T}^p$) acting on the capsule membrane are plotted as functions of the phase angle in the shear plane. Note that only the normal component of the fluid stress directly determines the capsule shape (see (3.1)–(3.3)), while the tangential component determines the tank-treading rotation of the capsule membrane. Previous studies on viscoelastic drops (Yue *et al.* 2005*b*; Aggarwal & Sarkar 2007) have pointed out that the tangential component of the

https://doi.org/10.1017/jfm.2018.88 Published online by Cambridge University Press

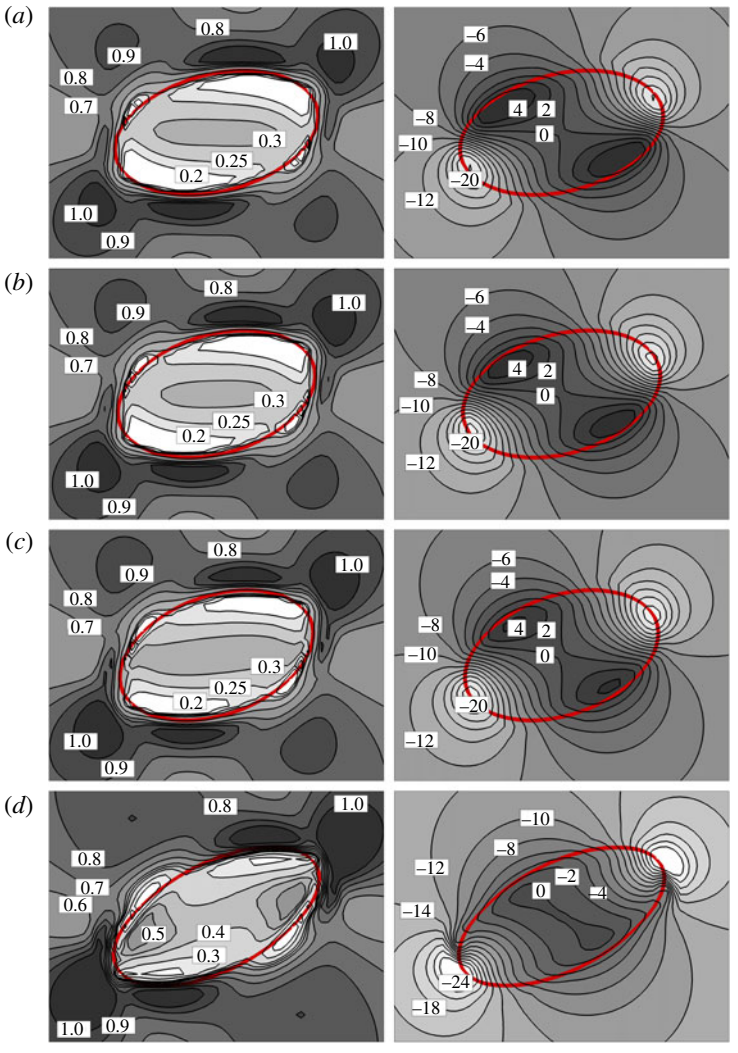


FIGURE 9. (Colour online) Contours of the strain rate (left panels) and pressure (right panels) for viscoelastic capsules in the steady state with different Deborah numbers, i.e. $De = 0.1$, 0.5, 1 and 10 in (*a–d*), respectively. Here, $Ca = 0.5$, $\mu^s_{in}/\mu_{out} = 1$ and $\lambda_\mu = 5$. The strain rate is calculated as $\|\boldsymbol{E}\| = (\boldsymbol{E} : \boldsymbol{E})^{1/2}$, where $\boldsymbol{E}$ is the strain rate tensor, i.e. $\boldsymbol{E} = (\nabla \boldsymbol{u} + \nabla \boldsymbol{u}^{\mathrm{T}})/2$. Note that the pressure values in the right panels are relative deviations from the pressure at capsule centre.

viscoelastic stress also has great effects on drop deformation, but these effects are generated indirectly via modifying the pressure that is one part of the normal fluid stress. Therefore, in our discussion, the normal component of the internal fluid stress is analysed in figures 8 and 10 to understand how *De* affects the capsule deformation, while the tangential component is analysed in figure 11 to understand the effects of *De* on the tank treading of the capsule membrane.

We first analyse the transient development of the fluid stress by presenting time evolution of the viscous and viscoelastic stresses in figure 8 for two different Deborah numbers, i.e. $De = 0.1$ and 1. When the relaxation time of the viscoelastic fluid is

https://doi.org/10.1017/jfm.2018.88 Published online by Cambridge University Press

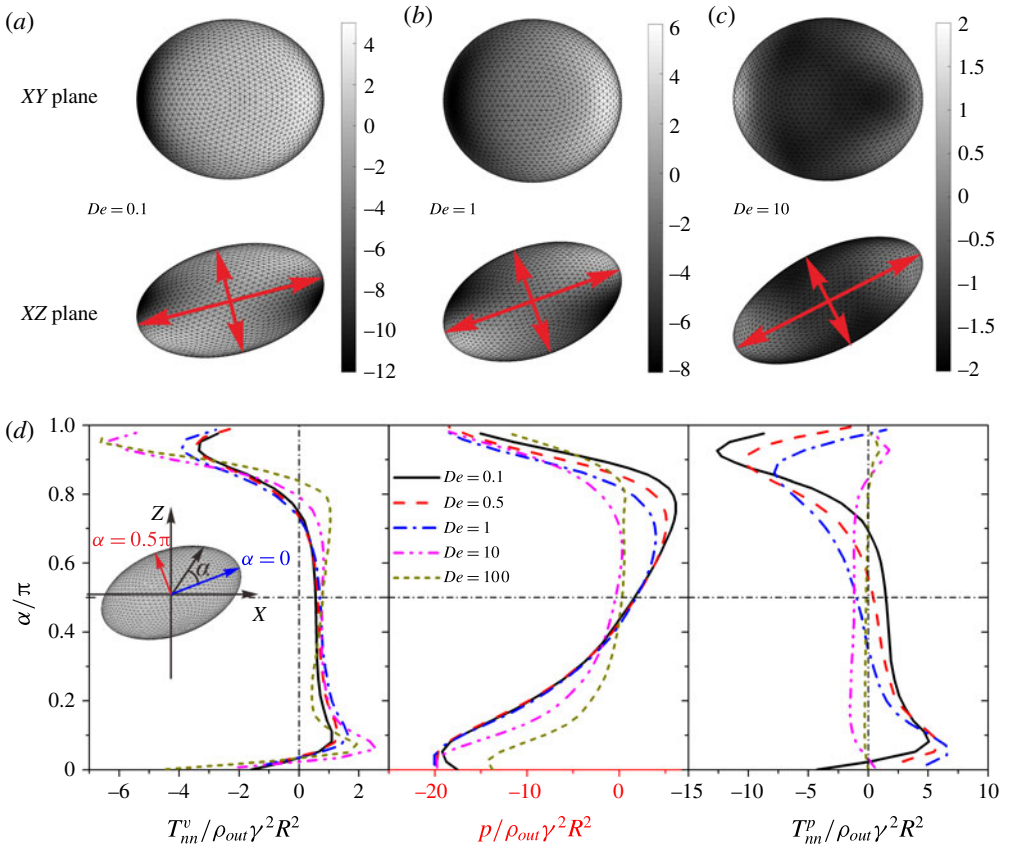


FIGURE 10. (Colour online) Normal stresses $T_{nn} = \boldsymbol{n} \cdot \boldsymbol{T} \cdot \boldsymbol{n}$ along the inner edge of the capsule membrane for different De at $Ca = 0.5$, $\mu^s_{in}/\mu_{out} = 1$ and $\lambda_\mu = 5$. (*a*)–(*c*) Three-dimensional contour plots of the normal viscoelastic stress. (*d*) The normal viscous stress, the pressure and the normal viscoelastic stress are plotted as functions of the phase angle α in the shear plane. The pressure values are relative deviations from the pressure at the centre point of the capsule.

quite small, the viscoelastic stress $\boldsymbol{T}^p$ develops quite fast and adapts rapidly to the changes in the shear strain $\boldsymbol{D}$, i.e. $\boldsymbol{T}^p \approx \mu^p \boldsymbol{D}$ (Yue *et al.* 2005*b*; James 2009). Besides, the distribution of the instantaneous viscous stress is representative of the distribution of the shear strain, i.e. $\boldsymbol{T}^v = \mu^s \boldsymbol{D}$. Therefore, the distribution of $\boldsymbol{T}^p$ tends to coincide with that of $\boldsymbol{T}^v$, while its value is approximately μ^p/μ^s times $\boldsymbol{T}^v$. As shown in figure 8(*a*) for $De = 0.1$ with $\mu^p_{in}/\mu^s_{in} = 4$, at each time frame, the magnitude of the viscoelastic stress is approximately four times that of the viscous stress, and the profiles are quite similar. It accounts for the same deformation of the viscoelastic capsule with $De = 0.1$ as that of the Newtonian capsule with the viscosity ratio of $(\mu^s_{in} + \mu^p_{in})/\mu_{out}$ (see figures 5–7). On the other hand, these results indicate that the internal viscoelastic stress plays the same primary role as the internal viscous stress does, which is to prevent the whole capsule deforming from the external fluid stress. However, when De is relatively high, the viscoelastic stress needs a finite time to develop fully. As shown in figure 8(*b*), for $De = 1$, $\boldsymbol{T}^p$ is smaller than that at $De = 0.1$ in the initial developing stage of the capsule deformation, though

https://doi.org/10.1017/jfm.2018.88 Published online by Cambridge University Press

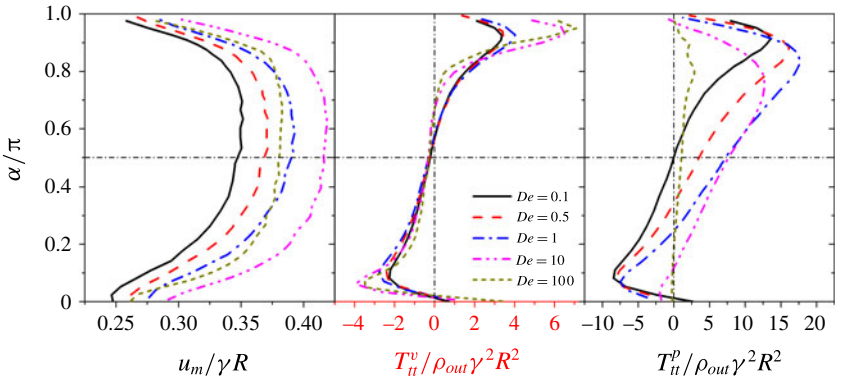


FIGURE 11. (Colour online) The membrane velocity, the tangential viscous stress and the tangential viscoelastic stress in the shear plane are plotted as functions of the phase angle. Tangential stresses are calculated as $T_{tt} = \boldsymbol{t} \cdot \boldsymbol{T} \cdot \boldsymbol{t}$, where $\boldsymbol{t}$ is a vector in the shear plane and tangential to the capsule membrane. Same parameter values are used as in figure 10.

they become close eventually when the capsule deformation reaches the steady state. Consequently, the capsule deforms more in the initial developing stage due to the reduced resistance from the viscoelastic stress, which is likely to induce overshoots in the capsule's transient deformation as shown in figure 4. Notably, this development of the viscoelastic stress in a finite time and the following overshoot in drop deformation is also observed in the numerical studies of viscoelastic drops (Yue *et al.* 2005*a*,*b*).

Next, we present a detailed discussion to understand the effects of the internal fluid viscoelasticity on the steady-state deformation of capsules. Previous studies on viscoelastic drops (Ramaswamy & Leal 1999; Yue *et al.* 2005*b*) have pointed out that the viscoelastic effect originates from two aspects, i.e. the direct impact of the viscoelastic stress at the drop interface and the flow modification induced by the viscoelastic stress. Specifically, via changing the pressure distribution at the drop interface, the flow modification effect makes the major contribution to the inhibition effect of the internal fluid viscoelasticity on the drop deformation in simple shear flow (Yue *et al.* 2005*b*; Aggarwal & Sarkar 2007). In figure 9, the distributions of both strain rate and pressure are presented at different Deborah numbers (i.e. $De = 0.1$, 0.5, 1 and 10) to examine the flow modification effect of the internal fluid viscoelasticity on the capsule deformation. In general, the strain rate inside the capsule is much smaller than that outside, since the flow inside is highly rotational while the external flow is a nearly simple shear flow. More importantly, as De increases, the distributions of both strain rate and pressure remain essentially identical to those of the Newtonian limit (i.e. $De = 0.1$), unless there is an obvious change in the shape and orientation of the whole capsule at large De (e.g. $De = 10$). Besides, as shown in figure 10(*d*), the magnitude and distribution of the normal viscous stress and the pressure exhibit insignificant change with increasing De unless the capsule shape is changed significantly at large De (e.g. $De = 10$ and 100). These results indicate that the internal fluid viscoelasticity induces no obvious change in the flow field; in other words, the flow modification effect of the viscoelastic stress is weak. Therefore, our following analysis focuses on the direct impact of the internal viscoelastic stress on the whole capsule deformation. Notably, the internal fluid viscoelasticity presents an inhibition effect at low De, but it shows a promotion effect at large De (see figures 5 and 7). Thus we discuss the underlying mechanisms separately through analysing the

https://doi.org/10.1017/jfm.2018.88 Published online by Cambridge University Press

normal component of the internal fluid stress acting on the capsule membrane (see figure 10).

With De increasing from 0 to $O(1)$ when the capsule deformation is inhibited, the distribution of the normal viscoelastic stress T^p_{nn} is altered remarkably while its magnitude shows insignificant change (see figure 10*d*). At $De = 0.1$ approximating the Newtonian limit (see figure 10*a*), the normal viscoelastic stress is tensile and pulls the membrane inward in the relatively large region upstream of the capsule poles (i.e. the end of the major axis). In contrast, it is compressive and pushes the membrane outward in the relatively small region downstream of the capsule poles. As De increases from 0.1 to 1 (see figure 10*b*,*d*), the distribution profile of T^p_{nn} shifts gradually as a whole along the same direction of the internal fluid rotation, while no shift is observed in the profile of T^v_{nn} that is representative of the shear strain. The origin of this shift in T^p_{nn} is attributed to the relaxation of the viscoelastic fluid. Thus there is a time lag between the shear strain and the viscoelastic stress in a steady flow, and increasing De implies a higher relaxation time leading to an increased time lag (Aggarwal & Sarkar 2007). Consequently, the maximum of T^p_{nn} shifts towards the capsule poles with its magnitude enlarged slightly, resulting in larger inward-pulling force in a very limited area around the poles. It tends to suppress capsule deformation at the poles, but the suppressing effect is weak. On the other hand, owing to the shift of the viscoelastic stress, it shows an obvious reduction in a much larger area around the capsule equator (i.e. the end of the minor axis). Moreover, the viscoelastic stress is even altered from the tensile state to the compressive state, which leads to larger outward-pushing force around the equator. This result indicates that the shift of the normal viscoelastic stress also tends to suppress capsule deformation at the equator, but the suppressing effect is stronger than that at the poles. In previous studies on viscoelastic drops (Yue *et al.* 2005*b*; Aggarwal & Sarkar 2007), the decrease of the drop deformation with De was also observed, and it is primarily attributed to the increased pressure at the drop equators. However, in our simulations for viscoelastic capsules, a small declination of the pressure is observed only downstream of the capsule poles, which makes little contribution to the suppressing effect on the whole capsule deformation; furthermore, its effect on the capsule deformation is offset by the alternated normal viscoelastic stress. To summarize, the declination of the normal viscoelastic stress in a large area around the capsule equator, which is caused by the relaxation-induced shift of the normal viscoelastic stress along the flow direction, is the major reason for the reduction of the capsule deformation at low De.

In the broad range of De from $O(1)$ to infinite when the capsule deformation is enlarged with De increasing, the shift of the normal viscoelastic stress profile is still observed. This is indicated clearly by the location shift of the maximum T^p_{nn} from the upstream to the downstream of the capsule poles (see figure 10*c*,*d*). However, another significant change in T^p_{nn} is the remarkable reduction of its magnitude with De increasing. As a result, the contribution of the viscoelastic stress to maintain the capsule's initial shape is greatly reduced, and the whole capsule deformation is therefore significantly enlarged. In fact, when De increases to very high values (e.g. $De = 100$), the viscoelastic stress turns out to be negligible compared with the viscous stress (see figure 10*d*); thus its contribution to the maintenance of the capsule shape vanishes eventually. This is consistent with both our simulation results shown in figures 5–7 and the expectation that the viscoelastic capsule with infinite De approximates the Newtonian limit with the viscosity ratio equivalent to the solvent viscosity ratio $(1-\beta)\lambda_\mu$ (see (3.3)).

To understand the significant effects of the internal fluid viscoelasticity on the tank-treading rotation of the capsule membrane (see figure 7*d*), the tangential

https://doi.org/10.1017/jfm.2018.88 Published online by Cambridge University Press

component of the internal fluid stress acting on the membrane is analysed (see figure 11), including the tangential viscous stress T_{tt}^{v} and the tangential viscoelastic stress T_{tt}^{p}. For all the cases of viscoelastic capsules, the tank-treading velocity of the membrane reaches its maximum and minimum at the equator and the poles respectively, which is similar to that for Newtonian capsules (Luo *et al.* 2015). With De increasing at low values, e.g. from 0 to $O(1)$, the tangential viscous stress presents little change, while the increasing relaxation time results in the shift of T_{tt}^{p} as a whole along the flow rotation direction. Consequently, T_{tt}^{p} shows an obvious increase in a large area around the capsule equators and hence increases the tank-treading velocity of the membrane, which accounts for the decrease of the tank-treading period with increasing De (see figure 7*d*). Note that the tangential viscoelastic stress has a positive value (i.e. has the same direction as the membrane tank treading) in most of the region, indicating the promotion effect of the viscoelastic stress on the membrane tank treading. However, similar to the changing tendency of the normal viscoelastic stress with increasing De, T_{tt}^{p} becomes negligible at high De, and hence its promotion effect becomes significantly weakened and eventually vanishes. This accounts for the reduced membrane velocity (figure 11) and the following increase of the tank-treading period at high De (figure 7*d*).

Finally, the mechanisms underlying the effects of the internal fluid viscoelasticity on the capsule orientation are also discussed. At $De = 0.1$ approximating the Newtonian limit (see figure 10), the internal viscoelastic stress pulls the membrane inward upstream of the capsule poles but pushes outward downstream of the poles; as a result, it provides a clockwise torque on the whole capsule. Therefore, the primary role of the internal viscoelastic stress is to rotate the capsule towards the flow direction and tend to decrease the capsule orientation θ; note that the internal viscous stress plays the same role. This accounts for the reduction of θ with λ_μ at low De (figure 7*c*), since the viscoelastic stress grows linearly with λ_μ. With De increasing, the shift of the viscoelastic stress and especially the rapid reduction of its magnitude strongly weaken its role in decreasing θ. As a result, θ increases significantly with De (figures 6 and 7*c*). Note that θ no longer exhibits obvious change at high De (i.e. $De = 5$–10), while the magnitude of the internal viscoelastic stress is still decreasing which is reflected in increasing capsule deformation. This is because the increased capsule deformation tends to decrease θ for low viscous capsules (Foessel *et al.* 2011), for example, θ decreasing with Ca (figure 6), and it counteracts the effect of decreasing viscoelastic stress at high De. Owing to the same reason, at large De (e.g. $De = 10$), θ increases slightly with λ_μ resulting from the decreased capsule deformation.

3.4. *Dynamics of non-spherical viscoelastic capsules*

As mentioned in the introduction, previous studies on Newtonian capsules have revealed that initially non-spherical capsules (either oblate or prolate) can present swinging or tumbling motion (Finken *et al.* 2011; Barthes-Biesel 2016). In these dynamical regimes, the shape and orientation of the capsule always show periodical oscillations and have no steady-state values, which differ significantly from those for initially spherical capsules exhibiting the tank-treading motion. In this section, we further investigate how the internal fluid viscoelasticity affects the deformation behaviours of non-spherical capsules exhibiting swinging or tumbling motion. Besides, the most important issue that previous studies on non-spherical Newtonian capsules have paid attention to is the transition between the tumbling and swinging motions.

https://doi.org/10.1017/jfm.2018.88 Published online by Cambridge University Press

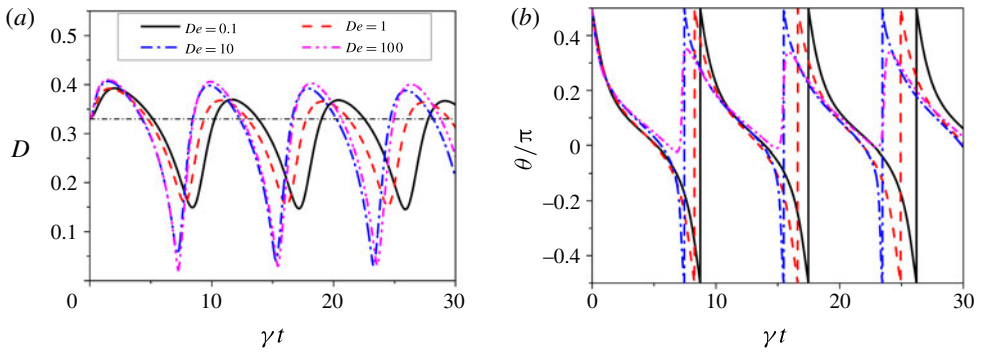


FIGURE 12. (Colour online) Effects of the internal fluid viscoelasticity on the dynamical motion of initially non-spherical capsules. (*a*) Transient deformation and (*b*) orientation of oblate capsules with $\lambda_\mu = 10$ at different De. Here, the aspect ratio a/b, the capillary number Ca and the internal solvent viscosity μ^s_{in}/μ_{out} are 0.5, 0.1 and 1, respectively.

This transition can be triggered via varying the viscosity ratio λ_μ, the capillary number Ca or the aspect ratio a/b of the capsule shape (Finken *et al.* 2011; Barthes-Biesel 2016). Therefore, we also examine if the internal fluid viscoelasticity (i.e. vary the Deborah number De) can trigger the tumbling-to-swinging transition and how De, λ_μ, Ca and a/b together affect the dynamical state transition of non-spherical viscoelastic capsules.

We find that the dynamical state of non-spherical viscoelastic capsules can be altered between tumbling and swinging via only varying the Deborah number. In figure 12, the time-dependent orientation angle θ and deformation index D are plotted for non-spherical capsules with different Deborah numbers (i.e. $De = 0.1$, 1, 10 and 100) but having the same parameters otherwise, i.e. $\lambda_\mu = 10$, $a/b = 0.5$, $Ca = 0.1$ and $\mu^s_{in}/\mu_{out} = 1$. At $De = 0.1$–10, the capsule exhibits the tumbling motion, as θ decreases periodically from $\pi/2$ to $-\pi/2$ indicating the complete rotation of the whole capsule. However, at $De = 100$, the capsule exhibits the swinging motion, since θ shows a periodic change (i.e. a periodic occurrence of a slow decrease and a rapid increase) with a variation smaller than $\pi/2$, indicating that the capsule's major axis swings up and down periodically. In the swinging motion, the capsule presents a periodic shape oscillation with much larger amplitude than those in the tumbling motion. Notably, during each oscillating period at $De = 100$, the major axis remains within the extensional quadrant of the flow (i.e. $0 < \theta < \pi/2$) for most of the time, while it may also enter the compressional quadrant (i.e. $-\pi/2 < \theta < 0$). Correspondingly, the deformation index D reaches its maximum and minimum when the capsule's major axis enters the extensional and compressional quadrants of the shear flow, respectively. Though similar motions are categorized more specifically as the transition regime in previous studies on Newtonian capsules (Bagchi & Kalluri 2009; Yazdani & Bagchi 2011), we categorize this motion as the swinging motion for simplicity. Furthermore, we find that the tumbling-to-swinging transition can be triggered by increasing the Deborah number alone regardless of the initial shape of the viscoelastic capsule, i.e. oblate or prolate (data not shown). Notably, the tumbling and swinging motions with the revolution axis in the shear plane are stable for oblate capsules but are unstable for prolate capsules, which has been pointed out in previous studies on Newtonian capsules (Cordasco & Bagchi 2013; Dupont *et al.* 2013, 2016).

https://doi.org/10.1017/jfm.2018.88 Published online by Cambridge University Press

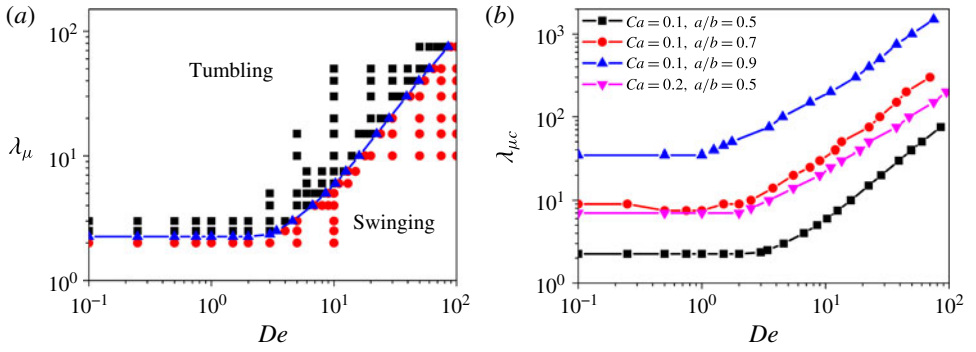


FIGURE 13. (Colour online) Effects of the internal fluid viscoelasticity on the tumbling-to-swinging transition of non-spherical capsules. (*a*) Phase diagram as a function of the viscosity ratio λ_μ and the Deborah number De. The solid line with symbols shows the tumbling-to-swinging transition. (*b*) Critical viscosity ratio of the tumbling-to-swinging transition as a function of the Deborah number De at different capillary numbers Ca or different aspect ratios a/b. Same parameter values are used as in figure 12.

Therefore, in the following analysis, we focus on the effects of the internal fluid viscoelasticity on the tumbling and swinging notions of an oblate capsule.

To further study the effects of the internal fluid viscoelasticity on the transition between swinging and tumbling, we have performed a large number of simulations with varying viscosity ratios λ_μ and Deborah number De. In figure 13(*a*), we plot a phase diagram showing the occurrence of swinging and tumbling as a function of λ_μ and De, which is restricted to an initially oblate capsule with $a/b = 0.5$, $Ca = 0.1$ and $\mu^s_{in}/\mu_{out} = 1$. In general, the tumbling motion is observed at large λ_μ and small De, whereas the swinging motion occurs at small λ_μ and large De. At very low Deborah number (i.e. $De = 0.1$) approaching the Newtonian limit with the viscosity ratio of λ_μ, the dynamical state of the capsule shifts from swinging to tumbling at a relatively low viscosity ratio (i.e. around 2.25). Notably, with De increasing, the critical viscosity ratio for the tumbling-to-swinging transition shows little change at low De from 0 to $O(1)$, but it shows an obvious increase at high De of $O(10–100)$. This observation can be explained by the fact that the magnitude of the viscoelastic stress undergoes little change at low De but decreases rapidly at high De (see figures 10 and 11). Once De is sufficiently large, the viscoelastic capsule is expected to behave nearly the same as the Newtonian limit with a viscosity ratio equivalent to μ^s_{in}/μ_{out}, e.g. exhibiting the swinging motion at $\mu^s_{in}/\mu_{out} = 1$; no matter how large the total viscosity ratio λ_μ is. From another perspective, when a viscoelastic capsule has μ^s_{in}/μ_{out} larger than the critical viscosity ratio of Newtonian capsules with same Ca and a/b, it follows that the capsule will invariably exhibit the tumbling motion regardless of the value of De and λ_μ. To investigate how De, λ_μ, Ca and a/b together affect the tumbling-to-swinging transition, we plot in figure 13(*b*) the critical viscosity ratio $\lambda_{\mu c}$ as a function of De at different a/b (i.e. 0.5, 0.7 and 0.9) or different Ca (i.e. 0.1 and 0.2). For all cases in figure 13(*b*), the capsule exhibits the tumbling motion above the curves (i.e. $\lambda_\mu > \lambda_{\mu c}$) while presents the swinging motion below the curves (i.e. $\lambda_\mu < \lambda_{\mu c}$). At each given value of De, $\lambda_{\mu c}$ increases with a/b or Ca, which is exactly same as that for Newtonian capsules in qualitative terms (Bagchi & Kalluri 2009; Barthes-Biesel 2016). On the other hand, for each case of Ca or a/b, $\lambda_{\mu c}$ always shows the same

https://doi.org/10.1017/jfm.2018.88 Published online by Cambridge University Press

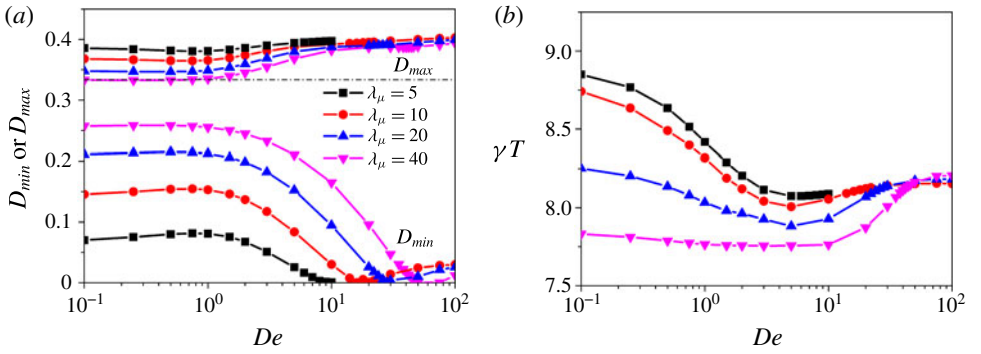


FIGURE 14. (Colour online) Effects of the internal fluid viscoelasticity on the deformation (*a*) and oscillating period (*b*) of non-spherical capsules in different dynamical regimes (i.e. swinging or tumbling). The dash-dot line represents the deformation index of the initially oblate shape with $a/b = 0.5$. The dynamical states of corresponding points can be found in figure 13(*a*) since the same parameter values are used.

qualitative changing tendency with De increasing: changing insignificantly below $O(1)$ but increasing remarkably with De within $O(1–100)$.

Finally, we present the effects of the internal fluid viscoelasticity on the deformation behaviours of non-spherical capsules exhibiting the swinging or tumbling motion. Since non-spherical capsules have no steady state but present periodic oscillations in their shapes (see figure 12), we plot the maximum and minimum values of the deformation index and the period of those oscillations as functions of the Deborah number in figure 14. When De increases at low values (e.g. $De < 1$), both D_{max} and D_{min} show little change for all given values of λ_μ. As De further increases to the tumbling-to-swinging transition, D_{max} shows a slight rise, but D_{min} rapidly decreases to 0. These results indicate the significant increase of the capsule deformation with increasing De. Note that the deformation of capsules in the tumbling regime shows a strong dependence on λ_μ. Once the capsule's dynamical state shifts to the swinging motion with De further increasing, D_{max} shows almost no change, and D_{min} slightly increases above 0; in other words, the capsule deformation shows very weak dependence on λ_μ. Similar to the changing tendency of the capsule deformation, the oscillating period γT (i.e. the period of tumbling or swinging) shows a strong dependence on λ_μ and De in the tumbling regime, while it presents no obvious change with varying λ_μ and De in the swinging regime (see figure 14*b*). These observations of the deformation behaviours of non-spherical capsules can be explained by the fact that the internal viscoelastic stress strongly depends on λ_μ at low De, but it decreases rapidly with increasing De and eventually approaches 0 at high De (see figures 10 and 11). Thus the internal viscoelastic stress makes little contribution to the determination of the capsule dynamics at high De, no matter how large λ_μ is.

4. Discussion and conclusion

In this paper, we study numerically the fundamental effects of the internal fluid viscoelasticity on the deformation and dynamics of an individual capsule freely suspended in a Newtonian fluid under simple shear. To this end, the Oldroyd-B constitutive equation governing the viscoelastic stress is integrated into the three-dimensional front-tracking finite-difference method that we previously developed

https://doi.org/10.1017/jfm.2018.88 Published online by Cambridge University Press

for purely Newtonian capsules. In contrary to most studies on viscoelastic drops, we employ an implicit scheme to discretize the convective term in the Oldroyd-B constitutive equation. Thus the effects of the internal fluid viscoelasticity are examined for a broad range of Deborah number, i.e. $De = 0$–$O(100)$. Our model is validated by quantitative agreement with previous numerical results on the deformation of Newtonian capsules and viscoelastic drops. Note that although our present model may be not applied to real world capsules directly, the findings obtained from this model regarding the fundamental effects of the internal fluid viscoelasticity could be helpful for further studying the flow dynamics of real capsules in engineering applications, which are summarized below.

The capsule dynamics is governed by the competition of the membrane stress and the internal and external fluid stresses, and previous studies have mainly focused on Newtonian fluid stress (Barthes-Biesel 2016). Here, we show that the viscoelastic stress may also play a significant role. Specifically, the internal viscoelastic stress plays the same primary role as the internal viscous stress, that is to prevent deformation of the whole capsule. Nevertheless, the effects of the internal viscoelastic fluid strongly depend on its relaxation time that can be characterized by the Deborah number De. At quite a small De (e.g. $De \leqslant 0.1$), the development of the viscoelastic stress is synchronized with the viscous stress, and hence the capsule deformation D approaches the Newtonian limit with $\lambda_\mu = (\mu^s_{in} + \mu^p_{in})/\mu_{out})$ that is $D = 5/4\lambda_\mu$ approximately for large viscosity ratios (Foessel *et al.* 2011). With De increasing, the capsule deformation decreases slightly (generally below 10 %) at low De (i.e. below $O(1)$), but it shows a much greater increase at high De (i.e. $O(1$–$100)$). At quite a large De (e.g. $De \geqslant O(100)$), the magnitude of the viscoelastic stress approaches 0 and hence the capsule deformation gradually approaches another Newtonian limit (i.e. $\lambda_\mu = \mu^s_{in}/\mu_{out}$). Recently, Raffiee, Dabiri & Ardekani (2017) also observed that the capsule deformation displays a non-monotonic behaviour with the Deborah number, although their study is limited to the viscosity-matched case with moderate De (i.e. $De \leqslant 8$).

One of the most important contributions of this study is that we unveil the mechanism underlying the effects of the internal fluid viscoelasticity on capsule deformation from the mechanical viewpoint. Actually, previous studies on viscoelastic drops under simple shear (as summarized in table 1) have also observed the reduction in drop deformation at low De. Ramaswamy & Leal (1999) pointed out that the viscoelastic effect may originate from two aspects, i.e. the direct impact of the viscoelastic stress at the drop interface and the flow modification induced by the viscoelastic stress. Yue *et al.* (2005*b*) and Aggarwal & Sarkar (2007) demonstrated that the inhibition effect of the internal fluid viscoelasticity on drop deformation is mainly due to the flow modification via changing the pressure distribution along the drop interface. However, for membrane-enclosed capsules, we find that the effects of the internal fluid viscoelasticity are mainly attributed to the direct impact of the viscoelastic stress at the capsule membrane while the viscoelasticity-induced flow modulation exerts a very weak effect. This difference between these two cases (i.e. drops and capsules) may result from the fact that the drop surface tension induces a large pressure jump across drop surface while there is no pressure jump across capsule membrane at the initial spherical state. This hypothesis may be verified via introducing an isotropic prestress into the membrane mechanics, which has been taken into account in a few studies on purely Newtonian capsules (Lac *et al.* 2004; Lac & Barthes-Biesel 2005).

Finally, we examine the principal effects of the internal fluid viscoelasticity on the unsteady dynamics of initially non-spherical capsules with a particular interest in the

https://doi.org/10.1017/jfm.2018.88 Published online by Cambridge University Press

tumbling-to-swinging transition. We have mainly considered an oblate capsule since the tumbling and swinging motions are stable for oblate capsules but are unstable for prolate capsules (Cordasco & Bagchi 2013; Dupont *et al.* 2013, 2016). Previous studies on Newtonian capsules have pointed out that the tumbling-to-swinging transition is governed by the viscosity contrast λ_μ, aspect ratio a/b and capillary number Ca. We demonstrate that for viscoelastic capsules the Deborah number De is another important parameter; specifically, the tumbling-to-swinging transition can be triggered by increasing De alone. In that respect, De has a similar effect on capsule dynamics as a/b, Ca or $1/\lambda_\mu$ does (Bagchi & Kalluri 2009). Besides, we find that with De increasing, the critical viscosity ratio for the tumbling-to-swinging transition has little change at low De but increases significantly at high De. The swinging motion can appear at high viscosity ratios, i.e. $\lambda_\mu = O(10\text{–}1000)$, as long as De is sufficiently large. In contrast, for Newtonian capsules, the swinging motion exists only at low λ_μ, i.e. below $O(10)$ (Finken *et al.* 2011). Notably, our results indicate the significant influence of the fluid viscoelasticity on capsule dynamics, although only the tumbling and swinging motions with the revolution axis remaining in the shear plane are concerned as a typical example. On the other hand, it is also of great interest to consider viscoelastic capsules with their revolution axis initially positioned off the shear plane, while it certainly requires much longer computational time (Cordasco & Bagchi 2013; Dupont *et al.* 2013, 2016).

As mentioned in the introduction, previous studies (see table 1 for relevant references) have focused on the motion and deformation of capsules enclosing a Newtonian fluid, which are helpful for understanding the flow dynamics of red blood cells or artificial liquid-core capsules (Freund 2014; Barthes-Biesel 2016). However, there are also many examples of capsules consisting of a viscoelastic fluid surrounded by a membrane, for instance, biological cells having an internal structure more complex than red blood cells (Tsai *et al.* 1993; Khismatullin & Truskey 2012), and artificial capsules enclosing a liquid core with biopolymers and other macromolecules or enclosing a gel core (Noble *et al.* 2004; Rożkiewicz *et al.* 2011; Huang *et al.* 2017). A fundamental question that arises at this point is whether the introduction of the fluid viscoelasticity confers new features on the flow dynamics of those viscoelastic capsules. In this study, we present a systematic investigation on the dynamics of capsules enclosing a viscoelastic fluid and show how the internal fluid viscoelasticity coupled with membrane mechanics produces a rich effect on the deformation and unsteady dynamics of those viscoelastic capsules. For example, the polymeric viscosity and the relaxation property of the internal viscoelastic fluid may significantly alter the deformation degree and the dynamical behaviour of the whole capsule; accordingly, the fluid viscoelasticity needs to be taken into account in the study of viscoelastic capsules under shear flows in real applications. Our findings are fundamental to better understand the motion and function of biological cells in physiological flow or in microfluidic applications and to help design and optimize those artificial capsules for cell encapsulation or substance transport. Nevertheless, when one uses the viscoelastic capsule model to any particular type of real applications, special attention needs to be paid to the choice of constitutive laws for the mechanics of both the membrane and the viscoelastic fluid. Our present numerical methodology based on the front-tracking finite-element method can be easily extended to consider other constitutive laws, such as the neo-Hookean law or the prestressed cortical shell model for the membrane, and the Giesekus relation or the incompressible Maxwell model for a viscoelastic fluid (Dong *et al.* 1988; Dong & Skalak 1992; Barthes-Biesel *et al.* 2002; Luo *et al.* 2014, 2015). It is

https://doi.org/10.1017/jfm.2018.88 Published online by Cambridge University Press

of future interest to study how the coupling of these constitutive laws affects the capsule dynamics in flows.

In this study, to reveal the effects of the internal fluid viscoelasticity on capsule dynamics from the fundamental viewpoint, we use dimensionless numbers including the capillary number Ca, the Deborah number De, the ratio of the internal to the external total viscosity λ_μ and the ratio of the polymeric to the total viscosity β of the internal fluid. Notably, these dimensionless numbers are actually linked to each other through physical dimensional parameters (see (2.13)). Most of our results are presented versus varying De while keeping β, Ca and λ_μ constant at several different values. These results show that changes in the physical properties of the capsule, especially the relaxation time and the polymeric viscosity of the internal fluid, have non-trivial effects on the deformation and dynamics of the whole capsule. On the other hand, when one considers a given capsule type, the capsule size R, the internal viscosity μ_{in}, the internal polymeric viscosity μ_{in}^p, the relaxation time of the internal viscoelastic fluid τ and the membrane mechanical property (e.g. E_s) are given. Then, Ca, De and λ_μ can be changed only via the shear rate γ and the external fluid viscosity μ_{out}, and this situation is actually very common in experimental studies or in real word applications. For leukocytes as an example, R, E_s and τ are approximately 5 μm, 100 μN m^{-1} and 0.2 s, respectively, and μ_{in} is usually much larger than μ_{out} (e.g. $\lambda_\mu > 1000$) (Khismatullin & Truskey 2012; Luo *et al.* 2014). According to our analysis in this study, when γ is low (i.e. both Ca and De are small), the viscoelastic capsule is equivalent to a Newtonian capsule; but its dynamics is dominated by the internal fluid stress over the membrane stress owing to high λ_μ. As a consequent, the capsule is hard to deform and hence can be modelled as a rigid sphere (Chang, Tees & Hammer 2000; Hammer 2014). However, when the shear rate γ becomes much larger (e.g. higher than 10^3 s^{-1}), both Ca and De may become sufficiently high. Accordingly, the capsule dynamics is governed by both the membrane stress and the fluid stress including the viscous and viscoelastic stresses, and hence both the complex membrane mechanics and the internal fluid viscoelasticity need to be taken into account. Therefore, our findings in this study could be helpful for the choice and development of appropriate mechanical models for white blood cells in shear flows.

Acknowledgements

This work was supported by the National Science Fund for Distinguished Young Scholars of China (Grant no. 51425603) and the Young Scientists Fund of the National Natural Science Foundation of China (Grant no. 51606146). Z.Y.L. was also supported by the Fundamental Research Funds for Central Universities of China (Grant no. xjj2016043).

REFERENCES

AGGARWAL, N. & SARKAR, K. 2007 Deformation and breakup of a viscoelastic drop in a newtonian matrix under steady shear. *J. Fluid Mech.* **584**, 1–21.

BAGCHI, P. & KALLURI, R. M. 2009 Dynamics of nonspherical capsules in shear flow. *Phys. Rev.* E **80**, 016307.

BAI, B. F., LUO, Z. Y., WANG, S. Q., HE, L., LU, T. J. & XU, F. 2013 Inertia effect on deformation of viscoelastic capsules in microscale flows. *Microfluid. Nanofluid.* **14**, 817–829.

BARTHES-BIESEL, D. 1980 Motion of a spherical microcapsule freely suspended in a linear shear flow. *J. Fluid Mech.* **100**, 831–853.

https://doi.org/10.1017/jfm.2018.88 Published online by Cambridge University Press

BARTHES-BIESEL, D. 2009 Capsule motion in flow: deformation and membrane buckling. *C. R. Phys.* **10**, 764–774.

BARTHES-BIESEL, D. 2011 Modeling the motion of capsules in flow. *Curr. Opin. Colloid Interface Sci.* **16**, 3–12.

BARTHES-BIESEL, D. 2016 Motion and deformation of elastic capsules and vesicles in flow. *Annu. Rev. Fluid Mech.* **48**, 25–52.

BARTHES-BIESEL, D., DIAZ, A. & DHENIN, E. 2002 Effect of constitutive laws for two-dimensional membranes on flow-induced capsule deformation. *J. Fluid Mech.* **460**, 211–222.

BARTHES-BIESEL, D. & RALLISON, J. M. 1981 The time-dependent deformation of a capsule freely sespended in a linear shear flow. *J. Fluid Mech.* **113**, 251–267.

CHANG, K.-C., TEES, D. F. & HAMMER, D. A. 2000 The state diagram for cell adhesion under flow: Leukocyte rolling and firm adhesion. *Proc. Natl Acad. Sci. USA* **97**, 11262–11267.

CHINYOKA, T., RENARDY, Y., RENARDY, M. & KHISMATULLIN, D. 2005 Two-dimensional study of drop deformation under simple shear for oldroyd-b liquids. *J. Non-Newtonian Fluid Mech.* **130**, 45–56.

CORDASCO, D. & BAGCHI, P. 2013 Orbital drift of capsules and red blood cells in shear flow. *Phys. Fluids* **25**, 091902.

DE LOUBENS, C., DESCHAMPS, J., EDWARDS-LEVY, F. & LEONETTI, M. 2016 Tank-treading of microcapsules in shear flow. *J. Fluid Mech.* **789**, 750–767.

DODSON, W. R. & DIMITRAKOPOULOS, P. 2009 Dynamics of strain-hardening and strain-softening capsules in strong planar extensional flows via an interfacial spectral boundary element algorithm for elastic membranes. *J. Fluid Mech.* **641**, 263–296.

DONG, C. & SKALAK, R. 1992 Leukocyte deformability: finite element modeling of large viscoelastic deformation. *J. Theor. Biol.* **158**, 173–193.

DONG, C., SKALAK, R., SUNG, K.-L. P., SCHMID-SCHONBEIN, G. & CHIEN, S. 1988 Passive deformation analysis of human leukocytes. *Trans. ASME J. Biomech. Engng* **110**, 27–36.

DUPONT, C., DELAHAYE, F., BARTHES-BIESEL, D. & SALSAC, A. V. 2016 Stable equilibrium configurations of an oblate capsule in simple shear flow. *J. Fluid Mech.* **791**, 738–757.

DUPONT, C., SALSAC, A. V. & BARTHES-BIESEL, D. 2013 Off-plane motion of a prolate capsule in shear flow. *J. Fluid Mech.* **721**, 180–198.

DUPONT, C., SALSAC, A. V., BARTHES-BIESEL, D., VIDRASCU, M. & LE TALLEC, P. 2015 Influence of bending resistance on the dynamics of a spherical capsule in shear flow. *Phys. Fluids* **27**, 051902.

FATTAL, R. & KUPFERMAN, R. 2005 Time-dependent simulation of viscoelastic flows at high weissenberg number using the log-conformation representation. *J. Non-Newtonian Fluid Mech.* **126**, 23–37.

FINKEN, R., KESSLER, S. & SEIFERT, U. 2011 Micro-capsules in shear flow. *J. Phys. Condens. Matter* **23**, 184113.

FOESSEL, E., WALTER, J., SALSAC, A. V. & BARTHES-BIESEL, D. 2011 Influence of internal viscosity on the large deformation and buckling of a spherical capsule in a simple shear flow. *J. Fluid Mech.* **672**, 477–486.

FORSYTH, A. M., WAN, J., OWRUTSKY, P. D., ABKARIAN, M. & STONE, H. A. 2011 Multiscale approach to link red blood cell dynamics, shear viscosity, and atp release. *Proc. Natl Acad. Sci. USA* **108**, 10986–10991.

FREUND, J. B. 2014 Numerical simulation of flowing blood cells. *Annu. Rev. Fluid Mech.* **46**, 67–95.

GUIDO, S. 2011 Shear-induced droplet deformation: effects of confined geometry and viscoelasticity. *Curr. Opin. Colloid Interface Sci.* **16**, 61–70.

HAMMER, D. A. 2014 Adhesive dynamics. *Trans. ASME J. Biomech. Engng* **136**, 021006.

HELFRICH, W. 1973 Elastic propeties of lipid bilayers: theory and possible experiments. *Z. Naturforsch.* C **28**, 693–703.

HUANG, H., YU, Y., HU, Y., HE, X., USTA, O. B. & YARMUSH, M. L. 2017 Generation and manipulation of hydrogel microcapsules by droplet-based microfluidics for mammalian cell culture. *Lab on a Chip* **17**, 1913–1932.

https://doi.org/10.1017/jfm.2018.88 Published online by Cambridge University Press

IZBASSAROV, D. & MURADOGLU, M. 2015 A front-tracking method for computational modeling of viscoelastic two-phase flow systems. *J. Non-Newtonian Fluid Mech.* **223**, 122–140.

IZBASSAROV, D. & MURADOGLU, M. 2016 A computational study of two-phase viscoelastic systems in a capillary tube with a sudden contraction/expansion. *Phys. Fluids* **28**, 012110.

JAMES, D. F. 2009 Boger fluids. *Annu. Rev. Fluid Mech.* **41**, 129–142.

KELLER, S. R. & SKALAK, R. 1982 Motion of a tank-treading ellipsoidal particle in a shear flow. *J. Fluid Mech.* **120**, 27–47.

KESSLER, S., FINKEN, R. & SEIFERT, U. 2008 Swinging and tumbling of elastic capsules in shear flow. *J. Fluid Mech.* **605**, 207–226.

KHISMATULLIN, D. B. & TRUSKEY, G. A. 2012 Leukocyte rolling on p-selectin: a three-dimensional numerical study of the effect of cytoplasmic viscosity. *Biophys. J.* **102**, 1757–1766.

KOLEVA, I. & REHAGE, H. 2012 Deformation and orientation dynamics of polysiloxane microcapsules in linear shear flow. *Soft Matt.* **8**, 3681–3693.

KOUMOUTSAKOS, P., PIVKIN, I. & MILDE, F. 2013 The fluid mechanics of cancer and its therapy. *Annu. Rev. Fluid Mech.* **45**, 325–355.

KWAK, S. & POZRIKIDIS, C. 2001 Effect of membrane bending stiffness on the axisymmetric deformation of capsules in uniaxial extensional flow. *Phys. Fluids* **13**, 1234–1242.

LAC, E. & BARTHES-BIESEL, D. 2005 Deformation of a capsule in simple shear flow: effect of membrane prestress. *Phys. Fluids* **17**, 072105.

LAC, E., BARTHES-BIESEL, D., PELEKASIS, N. A. & TSAMOPOULOS, J. 2004 Spherical capsules in three-dimensional unbounded stokes flows: effect of the membrane constitutive law and onset of buckling. *J. Fluid Mech.* **516**, 303–334.

LE, D. V. 2010 Effect of bending stiffness on the deformation of liquid capsules enclosed by thin shells in shear flow. *Phys. Rev.* E **82**, 016318.

LI, X. Y. & SARKAR, K. 2008 Front tracking simulation of deformation and buckling instability of a liquid capsule enclosed by an elastic membrane. *J. Comput. Phys.* **227**, 4998–5018.

LUO, Z. Y. & BAI, B. F. 2016 Dynamics of nonspherical compound capsules in simple shear flow. *Phys. Fluids* **28**, 101901.

LUO, Z. Y., HE, L. & BAI, B. F. 2015 Deformation of spherical compound capsules in simple shear flow. *J. Fluid Mech.* **775**, 77–104.

LUO, Z. Y., HE, L., WANG, S. Q., TASOGLU, S., XU, F., DEMIRCI, U. & BAI, B. F. 2014 Two-dimensional numerical study of flow dynamics of a nucleated cell tethered under shear flow. *Chem. Engng Sci.* **119**, 236–244.

LUO, Z. Y., WANG, S. Q., HE, L., XU, F. & BAI, B. F. 2013 Inertia-dependent dynamics of three-dimensional vesicles and red blood cells in shear flow. *Soft Matt.* **9**, 9651–9660.

MATSUNAGA, D., IMAI, Y., YAMAGUCHI, T. & ISHIKAWA, T. 2015 Deformation of a spherical capsule under oscillating shear flow. *J. Fluid Mech.* **762**, 288–301.

MUKHERJEE, S. & SARKAR, K. 2009 Effects of viscosity ratio on deformation of a viscoelastic drop in a newtonian matrix under steady shear. *J. Non-Newtonian Fluid Mech.* **160**, 104–112.

NI, M. J., KOMORI, S. & MORLEY, N. 2003 Projection methods for the calculation of incompressible unsteady flows. *Numer. Heat Transfer B-Fund.* **44**, 533–551.

NOBLE, P. F., CAYRE, O. J., ALARGOVA, R. G., VELEV, O. D. & PAUNOV, V. N. 2004 Fabrication of 'hairy' colloidosomes with shells of polymeric microrods. *J. Am. Chem. Soc.* **126**, 8092–8093.

OMORI, T., IMAI, Y., YAMAGUCHI, T. & ISHIKAWA, T. 2012 Reorientation of a nonspherical capsule in creeping shear flow. *Phys. Rev. Lett.* **108**, 138102.

POPEL, A. S. & JOHNSON, P. C. 2005 Microcirculation and hemorheology. *Annu. Rev. Fluid Mech.* **37**, 43–69.

POZRIKIDIS, C. 2001 Effect of membrane bending stiffness on the deformation of capsules in simple shear flow. *J. Fluid Mech.* **440**, 269–291.

RAFFIEE, A. H., DABIRI, S. & ARDEKANI, A. M. 2017 Deformation and buckling of microcapsules in a viscoelastic matrix. *Phys. Rev.* E **96**, 032603.

https://doi.org/10.1017/jfm.2018.88 Published online by Cambridge University Press

RAMANUJAN, S. & POZRIKIDIS, C. 1998 Deformation of liquid capsules enclosed by elastic membranes in simple shear flow: large deformations and the effect of fluid viscosities. *J. Fluid Mech.* **361**, 117–143.

RAMASWAMY, S. & LEAL, L. 1999 The deformation of a viscoelastic drop subjected to steady uniaxial extensional flow of a newtonian fluid. *J. Non-Newtonian Fluid Mech.* **85**, 127–163.

ROŻKIEWICZ, D. I., MYERS, B. D. & STUPP, S. I. 2011 Interfacial self-assembly of cell-like filamentous microcapsules. *Angew. Chem. Intl Ed. Engl.* **50**, 6324–6327.

SHRIVASTAVA, S. & TANG, J. 1993 Large deformation finite element analysis of non-linear viscoelastic membranes with reference to thermoforming. *J. Strain Anal. Eng.* **28**, 31–51.

SKALAK, R., TOZEREN, A., ZARDA, R. P. & CHIEN, S. 1973 Strain energy function of red blood cell membranes. *Biophys. J.* **13**, 245–280.

SUI, Y., CHEW, Y. T., ROY, P. & LOW, H. T. 2009 Inertia effect on the transient deformation of elastic capsules in simple shear flow. *Comput. Fluids* **38**, 49–59.

TAYLOR, G. I. 1934 The formation of emulsions in definable fields of flow. *Proc. R. Soc. Lond.* A **146**, 0501–0523.

TRYGGVASON, G., BUNNER, B., ESMAEELI, A., JURIC, D., AL-RAWAHI, N., TAUBER, W., HAN, J., NAS, S. & JAN, Y. J. 2001 A front-tracking method for the computations of multiphase flow. *J. Comput. Phys.* **169**, 708–759.

TSAI, M. A., FRANK, R. S. & WAUGH, R. E. 1993 Passive mechanical behavior of human neutrophils: power-law fluid. *Biophys. J.* **65**, 2078–2088.

UNVERDI, S. O. & TRYGGVASON, G. 1992 A front-tracking method for viscous, incompressible, multi-fluid flows. *J. Comput. Phys.* **100**, 25–37.

VERHULST, K., CARDINAELS, R., MOLDENAERS, P., AFKHAMI, S. & RENARDY, Y. 2009*a* Influence of viscoelasticity on drop deformation and orientation in shear flow. Part 2: dynamics. *J. Non-Newtonian Fluid Mech.* **156**, 44–57.

VERHULST, K., CARDINAELS, R., MOLDENAERS, P., RENARDY, Y. & AFKHAMI, S. 2009*b* Influence of viscoelasticity on drop deformation and orientation in shear flow: part 1. Stationary states. *J. Non-Newtonian Fluid Mech.* **156**, 29–43.

VILLONE, M. M., D'AVINO, G., HULSEN, M. A. & MAFFETTONE, P. L. 2015 Dynamics of prolate spheroidal elastic particles in confined shear flow. *Phys. Rev.* E **92**, 062303.

VLAHOVSKA, P. M., YOUNG, Y. N., DANKER, G. & MISBAH, C. 2011 Dynamics of a non-spherical microcapsule with incompressible interface in shear flow. *J. Fluid Mech.* **678**, 221–247.

WALTER, J., SALSAC, A. V. & BARTHES-BIESEL, D. 2011 Ellipsoidal capsules in simple shear flow: prolate versus oblate initial shapes. *J. Fluid Mech.* **676**, 318–347.

WANG, Z., SUI, Y., SPELT, P. D. M. & WANG, W. 2013 Three-dimensional dynamics of oblate and prolate capsules in shear flow. *Phys. Rev.* E **88**, 053021.

YAZDANI, A. & BAGCHI, P. 2011 Phase diagram and breathing dynamics of a single red blood cell and a biconcave capsule in dilute shear flow. *Phys. Rev.* E **84**, 026314.

YAZDANI, A. & BAGCHI, P. 2012 Three-dimensional numerical simulation of vesicle dynamics using a front-tracking method. *Phys. Rev.* E **85**, 056308.

YAZDANI, A. & BAGCHI, P. 2013 Influence of membrane viscosity on capsule dynamics in shear flow. *J. Fluid Mech.* **718**, 569–595.

YUE, P., FENG, J. J., LIU, C. & SHEN, J. 2005*a* Transient drop deformation upon startup of shear in viscoelastic fluids. *Phys. Fluids* **17**, 123101.

YUE, P., FENG, J. J., LIU, C. & SHEN, J. 2005*b* Viscoelastic effects on drop deformation in steady shear. *J. Fluid Mech.* **540**, 427–437.

ZANG, Y., STREET, R. L. & KOSEFF, J. R. 1994 A non-staggered grid, fractional step method for time-dependent incompressible Navier–Stokes equations in curvilinear coordinates. *J. Comput. Phys.* **114**, 18–33.

ZHANG, Y., YU, J., BOMBA, H. N., ZHU, Y. & GU, Z. 2016 Mechanical force-triggered drug delivery. *Chem. Rev.* **116**, 12536–12563.

ZHAO, M. Y. & BAGCHI, P. 2011 Dynamics of microcapsules in oscillating shear flow. *Phys. Fluids* **23**, 111901.

https://doi.org/10.1017/jfm.2018.88 Published online by Cambridge University Press